

# A conceptual model for glacial lake bathymetric distribution

Taigang Zhang<sup>1,2,3</sup>, Weicai Wang<sup>1</sup>, Baosheng An<sup>1,4</sup>

<sup>1</sup>State Key Laboratory of Tibetan Plateau Earth System, Environment and Resources (TPESER), Institute of Tibetan Plateau Research, Chinese Academy of Sciences, Beijing 100101, China

<sup>2</sup>College of Earth and Environmental Sciences, Lanzhou University, Lanzhou 730000, China

<sup>3</sup>Center for the Pan-Third Pole Environment, Lanzhou University, Lanzhou 730000, China

<sup>4</sup>School of Science, Tibet University, Lhasa 850011, China

**Correspondence:** Taigang Zhang (zhangtg16@lzu.edu.cn) and Weicai Wang (weicaiwang@itpcas.ac.cn)

**Abstract.** The formation and expansion of glacial lakes worldwide due to global warming and glacier retreat have been well documented in the past few decades. Thousands of glacial lake outburst floods (GLOFs) originating from moraine-dammed and ice-dammed lakes were reported, causing devastating impacts on downstream lives and properties. Detailed glacial lake bathymetry surveys are essential for accurate GLOF simulation and risk assessment. However, these bathymetry surveys are still scarce as glacial lakes located in remote and high-altitude environments hamper a comprehensive investigation. We developed a conceptual model for glacial lake bathymetric distribution using a semi-automatic simulation procedure. The basic idea is that the statistical glacial lake volume-area curves conform to a power-law relationship indicating that the idealized geometric shape of the glacial lake basin should be hemispheres or cones. First, by reviewing the evolution of various types of glacial lakes, we identified 9 standard conceptual models to describe the shape of lake basins. Second, we defined a general conceptual model to depict the continuum transitions between different standard conceptual models for those specific glacial lakes that lie between two standard conceptual models. Third, we nested the optimal conceptual model into the actual glacial lake basin to construct the water depth contours and interpolate the glacial lake bathymetric distribution. We applied the conceptual model to simulate six typical glacial lakes in the Third Pole with in-situ bathymetric surveys to verify the algorithm's applicability. The results show a high consistency in the point-to-point comparisons of the measured and simulated water depths with a total volume difference of approximately  $\pm 10\%$ . The conceptual model has significant implications for understanding glacial lake evolution and modeling GLOFs in the future.

## 29 **1 Introduction**

30 Globally, glacial recession and thinning have been well-documented over the last decades via field observations  
31 and remote sensing techniques (Yao et al., 2012; Zemp et al., 2019; Hugonnet et al., 2021). Such evolution of glaciers  
32 due to climate warming and anthropogenic factors could induce related effects (Yao et al., 2019), among which is the  
33 expansion and formation of glacial lakes (Zhang et al., 2015; Emmer et al., 2016; Wang et al., 2020; Ma et al., 2021).  
34 Glacial lakes are water bodies developed within depressions of glacier moraine or mainly fed by contemporary glacier  
35 meltwater (Yao et al., 2018). Due to glacier retreats, they are generally impounded by glacier terminal or lateral  
36 moraine. Since the 1990s, the glacial lakes within 1 km buffer of the contemporary glaciers worldwide have increased  
37 by around 50% in total number, area, and volume (Shugar et al., 2020). These changes have also been accompanied  
38 by glacial lake outburst flood (GLOF) risks.

39 As a glacier-related hazard, GLOF has been a frequent incidence in various glacierized areas, causing  
40 considerable socioeconomic losses (Anaconda et al., 2015a; Nie et al., 2018; Emmer et al., 2022a). According to a  
41 compilation, more than 3,000 GLOFs from moraine- and ice-dammed lakes are recorded worldwide and claim more  
42 than 10,000 deaths (Carrivick and Tweed, 2016; Lützow et al., 2023). Under the triggering factors such as ice  
43 avalanches, landslides, and heavy precipitation, glacial lakes are extremely unstable and subsequently cause a sudden  
44 release of water with peak discharge higher than a dozen times that of monsoon rainfall floods (Richardson and  
45 Reynolds, 2000; Westoby et al., 2014; Kougkoulos et al., 2018). However, due to the relatively small volume of the  
46 glacial lake, the flooding process generally attenuates rapidly within a few hours. Knowledge of glacial lake volume  
47 is critical, as it influences the released water volume and GLOFs magnitude (Fujita et al., 2013). Therefore, lake  
48 volume is often employed as an essential criterion in numerous cases of GLOF susceptibility and risk assessment  
49 (Bolch et al., 2011; Aggarwal et al., 2017; Drenkhan et al., 2019; Falatkova et al., 2019).

50 Currently, only sporadic bathymetric surveys on glacial lakes have been conducted worldwide. In Cordillera  
51 Blanca, Peru, facing continuous threats by GLOFs (Lliboutry et al., 1977), more than 100 detailed bathymetric  
52 surveys of glacial lakes have been carried out to better understand the regional GLOF risks (Muñoz et al., 2020).  
53 Government agencies and research institutions have promoted these surveys. In the Third Pole region, the bathymetric  
54 surveys are focused on the glacial lakes in the Himalayas (Sharma et al., 2018; Watson et al., 2018), where  
55 approximately 60 bathymetric surveys of glacial lakes, such as the Cirenmaco, Jialongco, and Longbasaba Lake,  
56 were conducted (Yao et al., 2012; Wang et al., 2018; Li et al., 2021). They measure the water depth with ultrasonic

57 devices onboard automatic uncrewed boats or manual hovercrafts.

58 Performing a universal investigation campaign of lake bathymetry is impractical for thousands of glacial lakes  
59 in remote areas and high elevations. Instead, scholars typically utilize single total lake volume data rather than  
60 bathymetric distribution in GLOF modeling (Anaconda et al., 2015b; Zhang et al., 2021). The lake volume is typically  
61 estimated by empirical equation, e.g., direct volume–area equation (O'Connor et al., 2001; Huggel et al., 2002;  
62 Loriaux and Casassa, 2013), or indirect area–mean depth/maximum depth/width equation (Wang et al., 2012), which  
63 have considerable uncertainty. There is no doubt that the measured and/or interpolated glacial lake bathymetric  
64 distribution have great merit that can precisely determine the maximum potential outburst volume of the glacial lake,  
65 serving to further simulate the GLOF propagation and evaluate downstream exposures (Frey et al., 2018; Sattar et  
66 al., 2021). Moreover, a bathymetry survey is also pivotal to understanding the interactions between the glaciers and  
67 their terminating lakes (Zhang et al., 2023), as several studies have revealed that the proglacial lake bathymetric state  
68 can dominate the glacier terminal melting and calving regimes (Watson et al., 2020; Sugiyama et al., 2021).

69 Can we obtain glacial lake bathymetric distributions through modeling rather than in situ investigations?  
70 Previous studies have provided insights. Cook and Quincey (2015) preliminarily proposed that the same type of  
71 glacial lakes may have their idealized geometric shapes, which depict the evolution of glacial lakes' volume–area (V–  
72 A) relationship over time. For instance, the triangular cone is suitable to represent the idealized geometric shape of  
73 ice-dammed lakes dammed by glaciers and formed in the narrow valley. The idealized conceptual models of glacial  
74 lakes can be combined with the actual situations to project the glacial lake bathymetric distribution.

75 An idealized lake basin is also helpful in constructing numerical or physical models. In the study of Veh et al.  
76 (2020), the conceptual model of glacial lakes was constructed as a semi-ellipsoid with a circular surface to calculate  
77 the released volume after the lake drainage. The surface area and height of the semi-ellipsoid refer to the glacier lake  
78 area and maximum water depth, respectively. Based on these instructive designs, we attempted to develop a procedure  
79 and algorithm for modeling glacial lake bathymetric distribution in this study. We first (i) retrieved as many as  
80 possible conceptual models for various types of glacial lakes by reviewing the evolutions of glacial lakes and  
81 analyzing the relationships between lake volumes and areas; (ii) explored the procedure and algorithm to estimate  
82 bathymetric distribution in conjunction with actual lake surface and basin shapes; and then (iii) discussed their  
83 implications and potential applications.

## 84 **2 Data and methods**

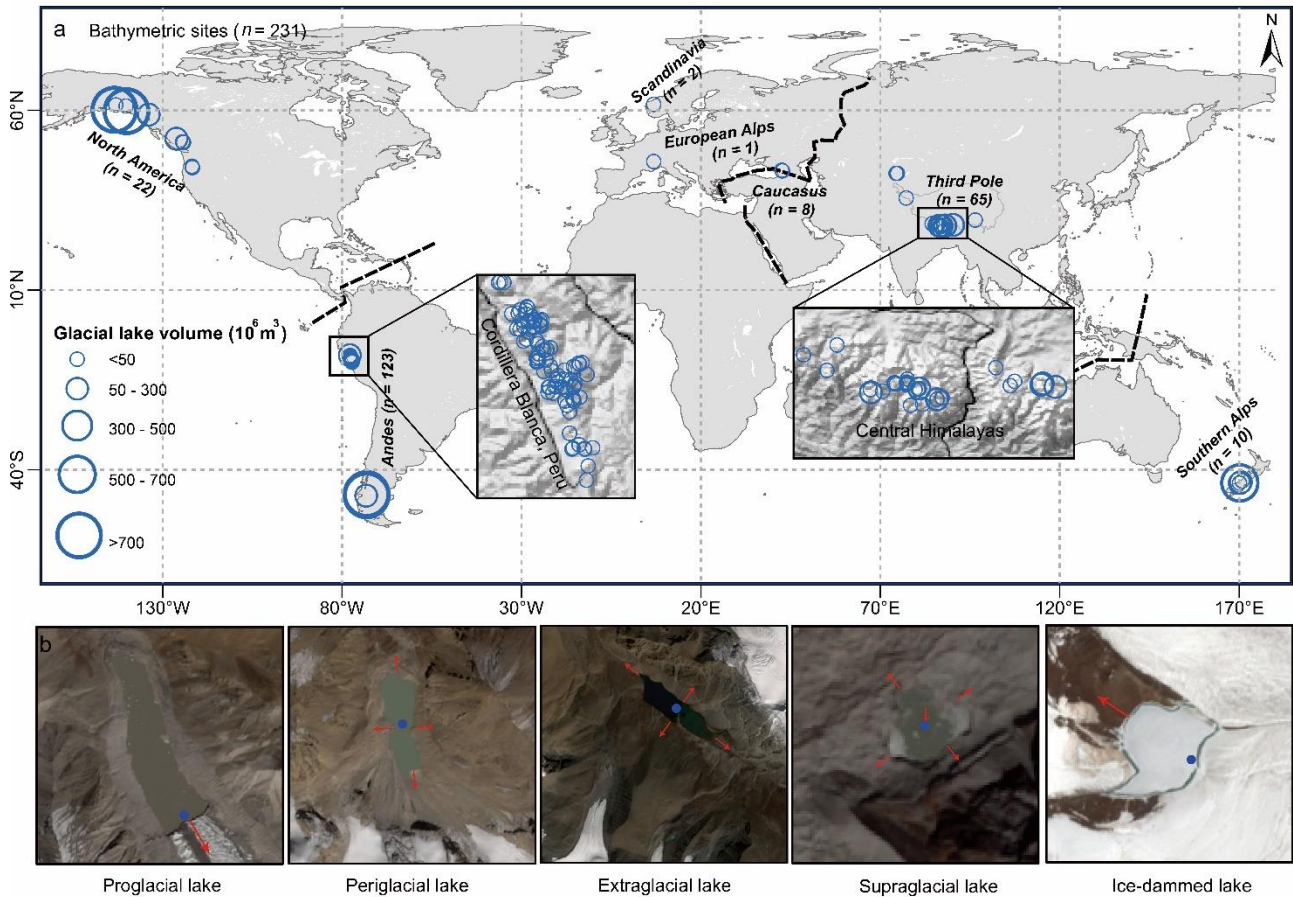
## 85 **2.1 Compilation of glacial lake bathymetry**

86 Analyzing the existing glacial lake bathymetries can help us reveal glacial lake water depth characteristics. To  
87 our knowledge, more than 60 articles have mentioned surveyed bathymetry data from glacial lakes. We integrated  
88 the prior studies and established an inventory of global glacial lake bathymetry (Supplementary material 1). The  
89 attributes included the name, location, survey time, area, volume, and maximum water depth. A total of 231  
90 bathymetric data from 220 glacial lakes globally were compiled in the inventory (Fig. 1a). Some large glacial lakes  
91 were eliminated since their area deviate from the majority of concentration zone which could reduce the fitting  
92 accuracy (Cook and Quincey, 2015).

## 93 **2.2 Classification and evolution of different glacial lake types**

94 The maximum water depth (D) and total volume (V) are the fundamental parameters regarding the idealized  
95 geometric shape of glacial lakes. We used the compiled glacial lake bathymetry data to fit the curves of V–A (glacial  
96 lake area) and D–A to understand the potential shapes of an idealized lake basin. Based on the topological positions  
97 between the glacial lakes and their parent glaciers, we classified glacial lakes as proglacial, periglacial, extraglacial,  
98 supraglacial, and ice-dammed types (Fig. 1b). This classification system considers glaciers' critical role in the  
99 evolution of glacial lakes (Petrov et al., 2017; Rick et al., 2022).

100 We assumed that different types of glacial lakes have different expansion mechanisms and, thus, different  
101 conceptual models. The proglacial lake's expansion mainly proceeds backward by glacial retreat. The periglacial lake  
102 and the extraglacial lake are not directly in contact with the glacier, and their expansion depends more on changes in  
103 precipitation and glacier meltwater, thereby potentially expanding in all horizontal directions. As for the supraglacial  
104 lake, expansion proceeds in all directions, and the temperature difference at the ice-water interface continuously melts  
105 the glacier ice in both horizontal and vertical orientations. While for ice-dammed lake, the evolution often appears  
106 horizontally with glacier retreat. These various mechanisms in glacial lake expansions showed that the changes in  
107 the lake basin among the different glacial lake types are inconsistent, indicating that they may have different  
108 conceptual models.



109

110

111

112

113

114

115

116

117

**Figure 1.** (a) Distribution of glacial lakes whose volume was surveyed in detail. (b) Glacial lakes were divided into five categories, namely proglacial (direct in contact with glacier terminus), periglacial (separated from the glacier and dammed by historical moraine), extraglacial (far from the glacier and generally dammed by landslides), supraglacial (positioned on the glacier surface), and ice-dammed lake (formed when glacier surges block downstream valleys or meltwater fills depressions between retreating tributary and main glaciers). Red arrows indicate the possible main directions of expansion of the glacial lake, and the blue points represent the location of maximum water depth.

### 2.3 Standard conceptual model

118

119

120

121

122

The basic procedure of constructing glacial lake bathymetric distribution is to (i) identify the most appropriate conceptual model that can describe the idealized lake basin, (ii) calculate the theoretical formulation equations of this conceptual model, (iii) nest this conceptual model into the actual glacial lake basin to construct the water depth contours, and (iv) interpolate and calculate the glacial lake bathymetric distribution. The conceptual model was constructed as the scheme presented by Veh et al. (2020). Glacial lakes were assumed to have hemispherical or similar

123 three-dimensional lake basin shapes. The standard surface of the glacial lake was assumed to be an ellipse.

124 The general formula between the volume and area of glacial lakes fits a power-law relationship (Table 1). It  
125 could be expressed as Eq. (1). The best-fit curve for the relationship between maximum water depth and area of  
126 glacial lakes also follows the power-law relationship (Eq. 2) (Fig. 2).

$$127 \quad V = \alpha A^\beta \quad (1)$$

$$128 \quad D = \gamma A^\varepsilon \quad (2)$$

129 A is the area of the glacial lake;  $\alpha$ ,  $\beta$ ,  $\gamma$ , and  $\varepsilon$  are the coefficients. The value of  $\beta$  is greater than 1, and  $\varepsilon$   
130 is less than 1.

131 The three-dimensional bodies representing the standard shape of a lake basin were required to have a general  
132 formula as defined by Eq. (3):

$$133 \quad V = \delta AD \quad (3)$$

134 Here,  $\delta$  is the coefficient, A is the elliptical surface area, and D corresponds to the maximum water depth of  
135 the glacial lake. We identified four hemispheres or cones whose volumes can be expressed by Eq. (3): the hemisphere  
136 structured by the elliptical side ( $V = 2/3AD$ ); the hemisphere structured by the upward-opening parabolic side ( $V =$   
137  $1/2AD$ ); the cone structured by the straight side ( $V = 1/3AD$ ); and the cone structured by the rightward-opening  
138 parabolic side ( $V = 1/5AD$ ). These bodies are defined as the standard conceptual model (SCM), and their curves in  
139 the X-O-Z quadrant are called the standard curves (Fig. 3a). These four standard curves are progressively concave  
140 inward in the quadrant, from the elliptical curve to the rightward-opening parabolic curve.

141 These SCMs for the supraglacial, periglacial, and extraglacial lakes are compatible with the expansion  
142 mechanisms partly because their growth direction is comprehensive at the horizontal level. Their maximum water  
143 depths were set in the lake center. However, proglacial and ice-dammed lakes are different. Their expansions are  
144 focused toward the glacier's or valley's direction, and the maximum water depths are generally situated near the  
145 intersection with the glacier. Under these circumstances, we considered the SCMs of proglacial lakes to be half of  
146 the preceding four SCMs, namely the semi-hemisphere structured by the elliptical side ( $V = 1/3AD$ ); the semi-  
147 hemisphere structured by the upward-opening parabolic side ( $V = 1/4AD$ ); semi-cone structured by the straight side  
148 ( $V = 1/6AD$ ); and the semi-cone structured by the rightward-opening parabolic side ( $V = 1/10AD$ ). We designed two  
149 SCMs for the ice-dammed lake (Fig. 3a): the semi-cone structured by the straight side ( $V = 1/6AD$ ) and the triangular

150 cone ( $V = 1/3AD$ ). The deepest point for proglacial and ice-dammed lake were set near the glacier-lake interface.  
 151 Most of the actual volume points lie between the volume curves of these SCMs (Fig. 4), and there are one or two  
 152 closer SCM volume curves for each type of glacial lake's fitted A–V curve. Ultimately, a total of 9 different SCMs  
 153 were designed to express the idealized geometric shapes of glacial lake basin.

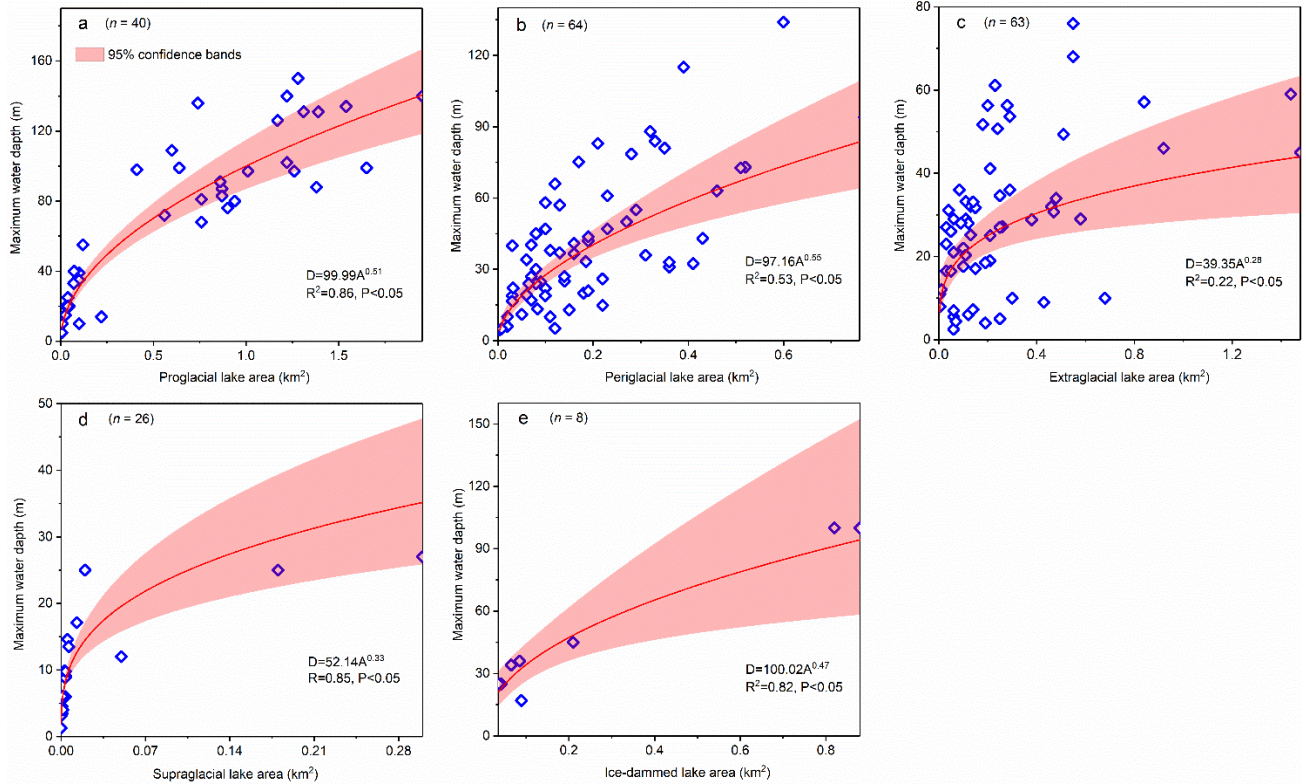
154

155 **Table 1.** Empirical equations of volume and area of glacial lakes in previous studies. The applicable region, lake type, and sample size  
 156 for each empirical equation were indicated during fitting. The volume unit is  $10^6 \text{ m}^3$ , and the area unit is  $\text{km}^2$ . In the dam material-  
 157 based classification method for glacial lakes, a substantial number of proglacial and periglacial lakes can be categorized as moraine-  
 158 dammed lakes.

ID	Empirical formulas	Region	Lake types	Samples	Reference
1	$V = 35A^{1.5}$	British Columbia, Canada	Ice-dammed lake	not mentioned	Evans, 1986
2	$V = 168.5A^2 + 3.11A$	Northwestern America	Moraine-dammed lake	7	O'Connor et al., 2001
3	$V = 34.44A^{1.42}$	Worldwide	Moraine- and ice-dammed lake	13	Huggel et al., 2002
4	$V = 43.24A^{1.53}$	Himalayas	Moraine-dammed lake	17	Sakai, 2012
5	$V = 6.07A^{1.37}$	Himalayas	Moraine-dammed lake	20	Wang et al., 2012
6	$V = 55A^{1.25}$	Himalayas	Moraine-dammed lake	20	Fujita et al., 2013
7	$V = 33.58A^{1.39}$	Worldwide	Moraine- and ice-dammed lake	31	Loriaux and Casassa, 2013
8	$V = 42.93A^{1.48}$	Peruvian Andes	Moraine- and bedrock-dammed lake	35	Emmer and Vilímek, 2014
9	$V = 34.07A^{1.37}$	Worldwide	Various types	69	Cook and Quincey, 2015
10	$V = 11.49A^{1.26}$	Worldwide	Supraglacial lake	9	Cook and Quincey, 2015
11	$V = 60A - 6.28$	Worldwide	Moraine-dammed lake	42	Cook and Quincey, 2015
12	$V = 2.63e^A$	Worldwide	Ice-dammed lake	9	Cook and Quincey, 2015
13	$V = 37.3A^{1.47}$	Himalayas	Moraine-dammed lake	33	Khanal et al., 2015
14	$V = 52.2A^{1.18}$	Himalayas	Proglacial lake	6	Sharma et al., 2018
15	$V = 40A^2 + 5.06A$	Himalayas	Moraine-dammed lake	17	Patel et al., 2017
16	$V = 35.36A^{1.47}$	Central Asia	Moraine-dammed lake	32	Kapitsa et al., 2017
17	$V = 32.13A^{1.49}$	Himalayas	Ice-dammed lake, supraglacial lake	not mentioned	Miles et al., 2018
18	$V = 28.95A^{1.33}$	Worldwide	Moraine-dammed lake	93	Watson et al., 2018
19	$V = 35.46A^{1.4016}$	Himalayas	Supraglacial lake	24	Watson et al., 2018
19	$V = 41WA + 2A$	Cordillera Blanca, Peru	Moraine-dammed lake	120	Muñoz et al., 2020
20	$V = 37.36A^{1.41}$	Peruvian Andes	Various types	170	Wood et al., 2021
21	$V = 38.04A^{1.36}$	Peruvian Andes	Moraine-dammed lake	not mentioned	Wood et al., 2021
22	$V = 43.27A^{1.64}$	Peruvian Andes	Unclassified	not mentioned	Wood et al., 2021

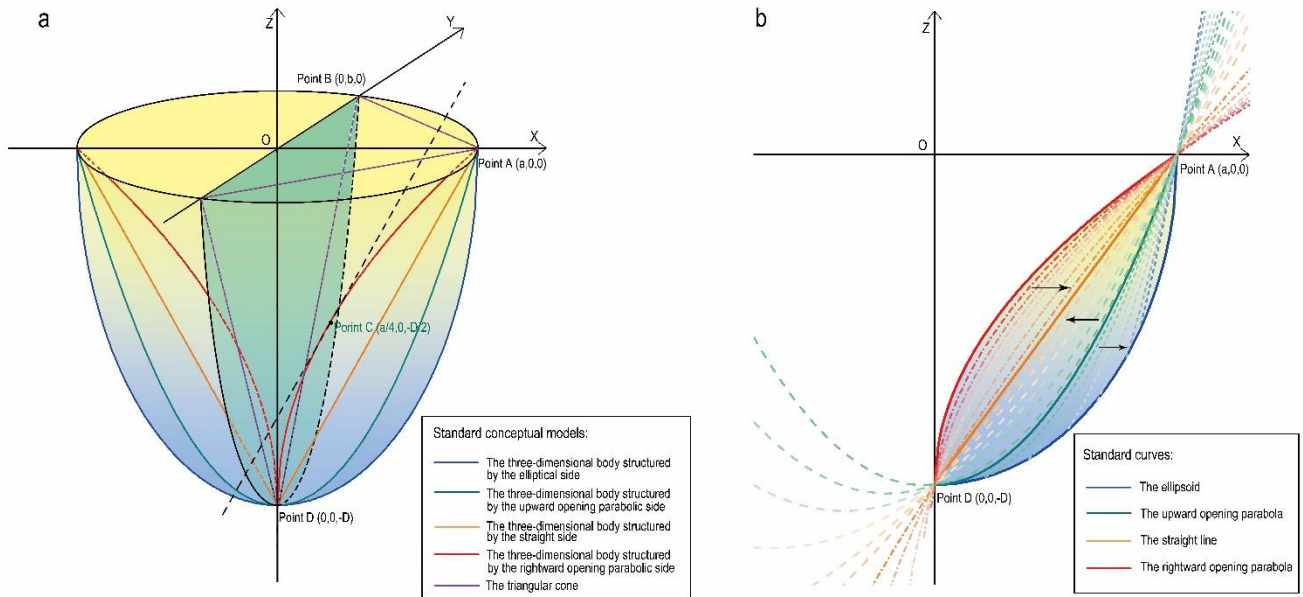
159





160

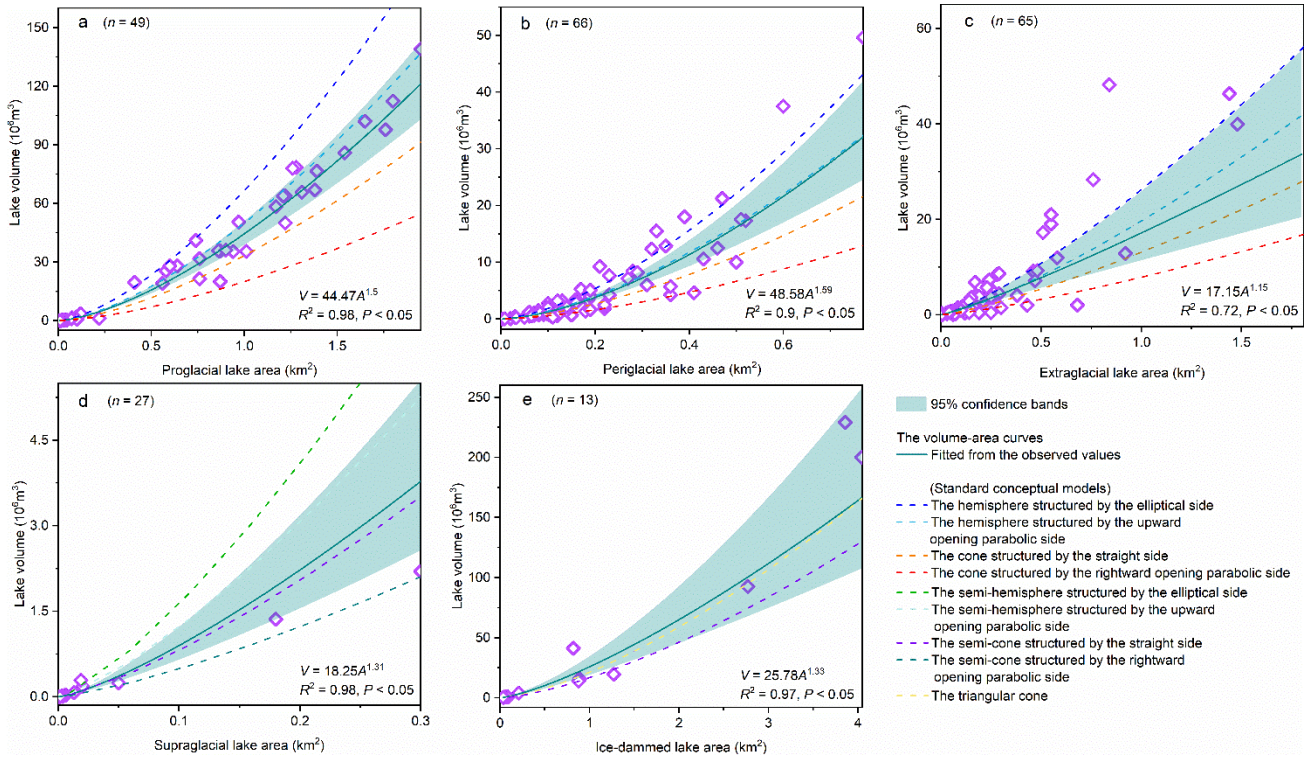
161 **Figure 2.** Relationships between maximum water depth and the area of glacial lakes were compiled in the present study for the following  
 162 lake types: (a) proglacial lake, (b) periglacial lake, (c) extraglacial lake, (d) supraglacial lake, and (e) ice-dammed lake.



163

164 **Figure 3.** (a) Schematic diagram illustrates the shapes of the SCMs, namely the hemisphere structured by the elliptical side/upward-  
 165 opening parabolic side, the cone D structured by the straight side/rightward-opening parabolic side, the triangular cone, as well as their  
 166 shapes when symmetrically divided matching the SCMs of the proglacial lake. Here, A is the semi-long axis, B is the elliptical surface's  
 167 semi-short axis, and D is the maximum water depth. (b) Convergences of the general curves towards the standard curves in the X–O–Z





169

170 **Figure 4.** Relationships between the volume ( $V$ ) and area ( $A$ ) of glacial lakes were compiled in the present study for the following lake  
 171 types: (a) proglacial lake, (b) periglacial lake, (c) extraglacial lake, (d) supraglacial lake, and (e) ice-dammed lake. The dotted lines  
 172 indicate the volume curves of different standard conceptual models, which were fitted by Eq. (2) and (3).

173 **2.4 General conceptual model**

174 If a specific glacial lake has determined its parameters such as surface size, maximum water depth, and volume,  
 175 it is unlikely that the closest SCM would accurately represent the most appropriate conceptual model. This is because  
 176 the relatively inherent volume of the SCM is hardly equal to the volume of a specific glacial lake. In other word, the  
 177 volume curve of the SCM is constant, and therefore, the volume point of a specific glacial lake may deviate from the  
 178 SCM volume curve. Consequently, directly using the SCM to nest and interpolate a realistic glacial lake bathymetric  
 179 distribution would result in an initial over- or underestimation of the total lake volume.

180 The SCMs can only help us comprehend the various glacial lake morphologies; they cannot be applied directly  
 181 to estimate the glacial lake bathymetric distribution. We may conceive the measured volume points between the SCM  
 182 volume curves as a result of the transition from one SCM to another. For instance, from the upward-opening parabolic  
 183 line to the straight line, it is the standard parabolic line continuously approximating the straight line on the X–O–Z

184 quadrant by moving downward and left (Fig. 3b). During the movement process, the rotated-out hemisphere is  
185 moving toward the cone structured by the straight side. We can capture these general conceptual models (GCMs) in  
186 this transition stage and make their volume consistent with the measured or estimated lake volume. This means we  
187 find a GCM that is more effective than the SCM in estimating the lake depth distribution.

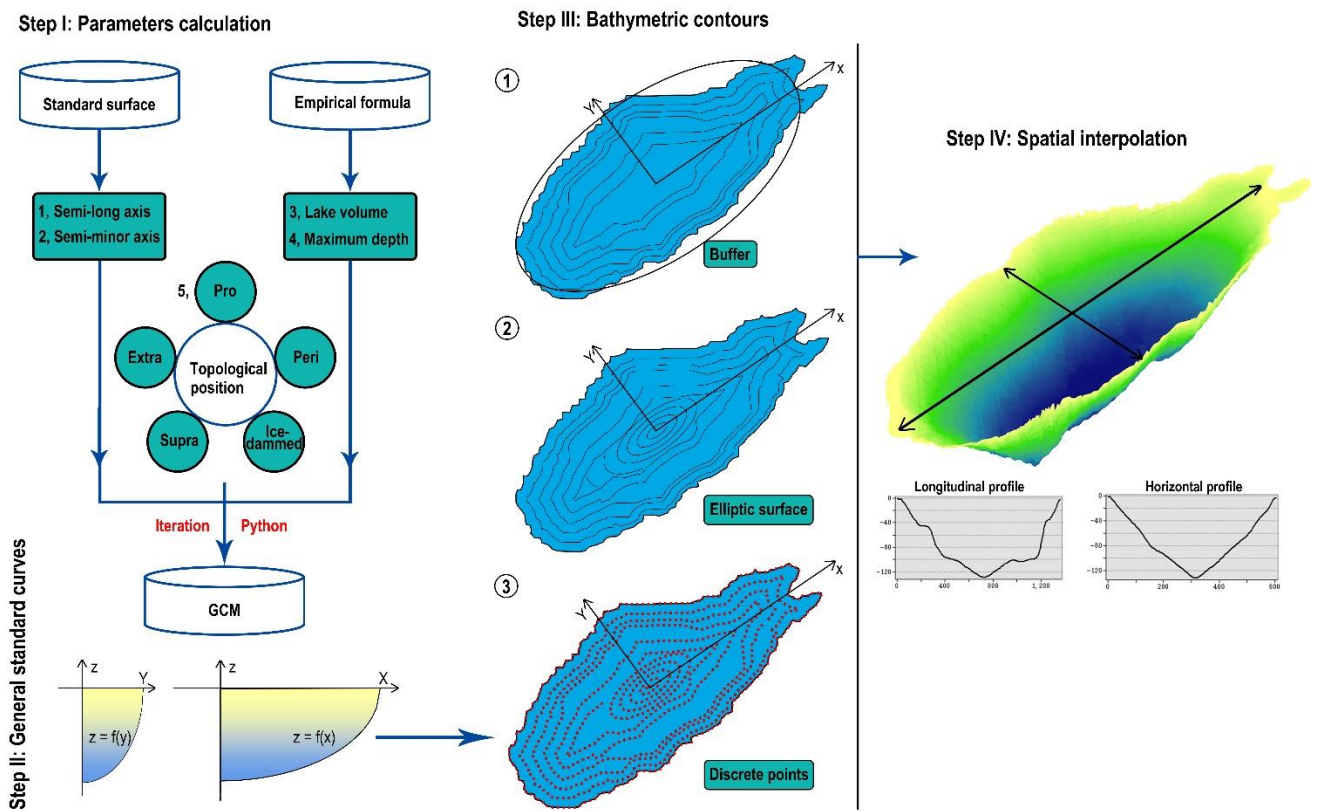
188 Python programming was used to drive the standard curves' transition and parameter calculations. The  
189 theoretical description for the GCMs is presented in supplementary material 2. By relocating the standard curve's  
190 vertices and altering the opening size, it is simple to compute the transition of a standard upward/rightward-opening  
191 parabola to a straight line. The resultant general curves must pass through points A and D. The convergence to the  
192 standard elliptic curve from the standard upward-opening parabola is relatively complicated. If we move the vertices  
193 of the standard parabola to the right and downward, the maximum height of the produced GCM changes. We used a  
194 compound style here. When the second intersection of the moved general parabolic curve and the standard elliptic  
195 curve occurs (from right to left), the side of GCM starts to take the elliptic curve change. Additionally, the marginal  
196 SCMs should be employed when the measured volume is larger (smaller) than the largest (smallest) SCM volume.

## 197 **2.5 Nesting the actual glacial lake shapes**

198 Once a given glacial lake's GCM has been established, the lake's bathymetric contours may be predicted in  
199 relation to actual conditions and parameters. Since the actual shape of the glacial lake surface is irregular, rather than  
200 the normal elliptic surface we used in the models, it was crucial to determine how the depth contours move inward  
201 based on the actual shape.

202 We tested two hypotheses. First, utilizing the lakeshore line to continually create buffers inward might depict  
203 the depth contours because the depth contours near the lakeshore were the consequence of ongoing indentation of the  
204 actual glacial lake surface outline inward. Second, at the 1/4 semi-long axis of the standard elliptic surface, the depth  
205 contours would become progressively blurred as the inward indentation continues, thus subsequently using the  
206 standard elliptic surface to start the inward indentation (Fig. 5). Importantly, these assumptions were supported by  
207 observations of hundreds of glacial lake bathymetric distribution cases worldwide. Some similarities exist between  
208 the bathymetric contours and the lakeshore shape, suggesting that the area near the lakeshore is possibly impacted by  
209 the slopes around the lake and/or other material sources. There are two explanations for this phenomenon: either the  
210 glacial lakes were continuously filled with exogenous debris and rocks, or the initial lake water level had risen and  
211 flooded part of the original slopes.

212 The 1/4 semi-long axis is the ending position where the glacial lake is not impacted by exogenous materials, as  
 213 determined by our understanding of those SCMs. Most of the glacial lake SCMs were located closer to the cone,  
 214 structured by the straight side of the hemisphere and the upward-opening parabolic side. It is inferred that the initial  
 215 deepening of the glacial lake is not particularly large from the outer line to the center (compared to the semi-ellipsoid),  
 216 indicating that exogenous materials are likely to have impacted it. This situation is better understood when the lake  
 217 SCM is a cone structured by the rightward-opening parabolic side. Therefore, we hypothesized an extreme  
 218 circumstance in which a glacial lake starts to be significantly influenced by the lake's surroundings' topography. In  
 219 this case, the slope of the standard rightward-opening parabolic curve is smaller than the slope of the standard straight  
 220 line and closer to the ideal deepening state of the lake basin when it is larger. This equal slope point is located at the  
 221 1/4 semi-long axis and represents half of the maximum water depth.



222  
 223 **Figure 5.** The procedure illustrates the parameter calculation of GCMs and processes of creating buffers inward. The water depths on  
 224 the axes were calculated using the standard curves corresponding to the X and Y axes.

225 **2.6 Sites for exhibiting and validating results**

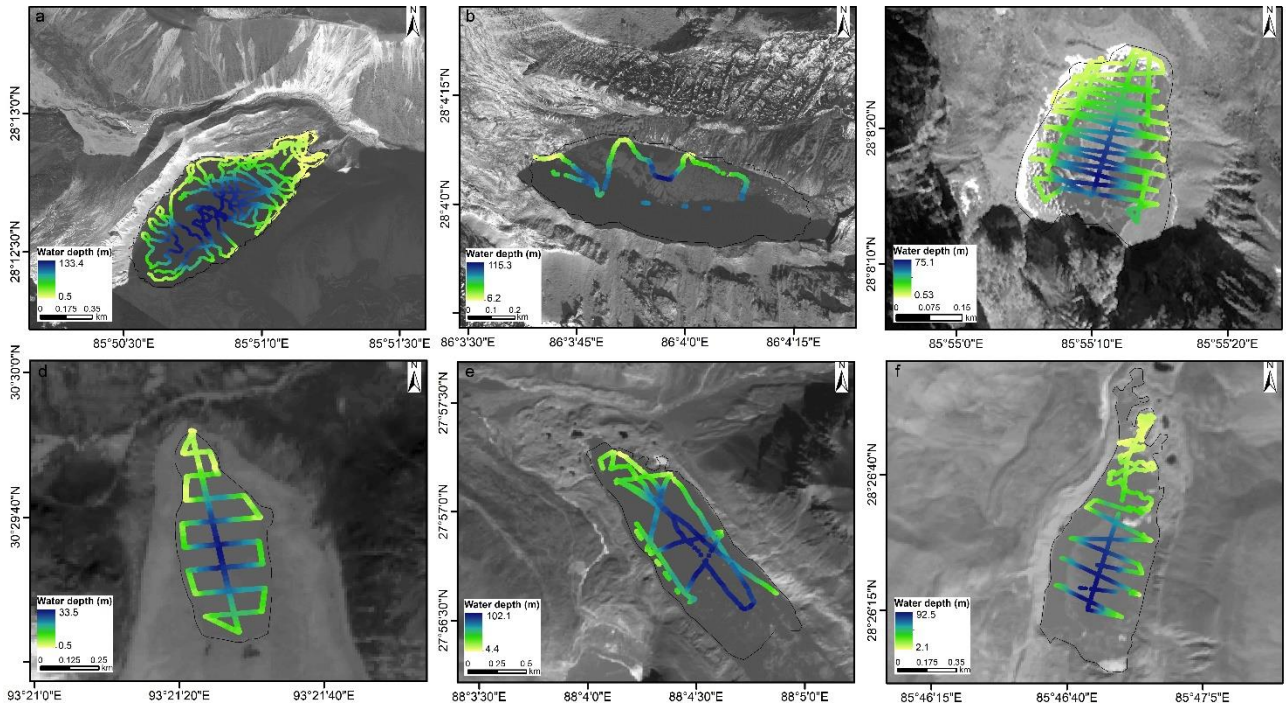
226 Six sets of bathymetry data were collected for the typical glacial lakes in the Himalayas and Nyainqentanglha  
 227 (Fig. 6). Among them, Jialongco, Cirenmaco, Poiqu NO.1, and Maqiongco were classified as periglacial lakes, while

228 the Longbasaba Lake and Dasuopuco were classified as proglacial lakes. Although it would be desirable to evaluate  
 229 the performance of our conceptual models across different types, sizes, and geographic locations of glacial lakes, we  
 230 were limited by the available observational data and could only conduct these examinations in the Third Pole region,  
 231 focusing on proglacial and periglacial lake types. The topological position, total volume, maximum water depth, and  
 232 semi-long/minor axis of the standard lake surface were crucial parameters in glacial lake bathymetric distribution  
 233 modeling (Table 2). The six glacial lake bathymetric distributions were simulated according to the lake sizes in the  
 234 survey year and eventually compared with the measured points of water depths and the overall parameters (total  
 235 volume and mean water depth) to verify the feasibility and accuracy of our modeling method.

236 **Table 2.** The crucial modeling parameters of the six selected glacial lakes.

Name	Lat°	Lon°	Region	Topological position	Survey year	Area (km <sup>2</sup> )	Volume (10 <sup>6</sup> m <sup>3</sup> )	Mean water depth (m)	Maximum water depth (m)	Semi-long axis (m)	Semi-minor axis (m)
Jialongco	28.21	85.85	Central Himalaya	periglacial	2020	0.61	37.5	58.2	133	757	314
Cirenmaco	28.07	86.07	Central Himalaya	periglacial	2012	0.33	18.0	55	115	549	185
Poiqu NO.1	28.14	85.92	Central Himalaya	periglacial	2021	0.11	2.7	25.5	75.1	242	129
Maqiongco	30.49	93.36	Nyainqentanglha	periglacial	2021	0.23	3.2	15	33.5	493	168
Longbasaba Lake	27.95	88.08	Eastern Himalaya	proglacial	2009	1.17	64.0	48	102	1949	319
Dasuopuco	28.44	85.78	Central Himalaya	proglacial	2021	0.55	0.55	33.8	93	1362	247

237



238

239 **Figure 6.** The water depth observed along the bathymetric routes for (a) Jialongco, (b) Cirenmaco, (c) Poiqu NO.1, (d) Maqiongco, (e)



240 Longbasaba Lake, and (f) Dasuopuco.

241

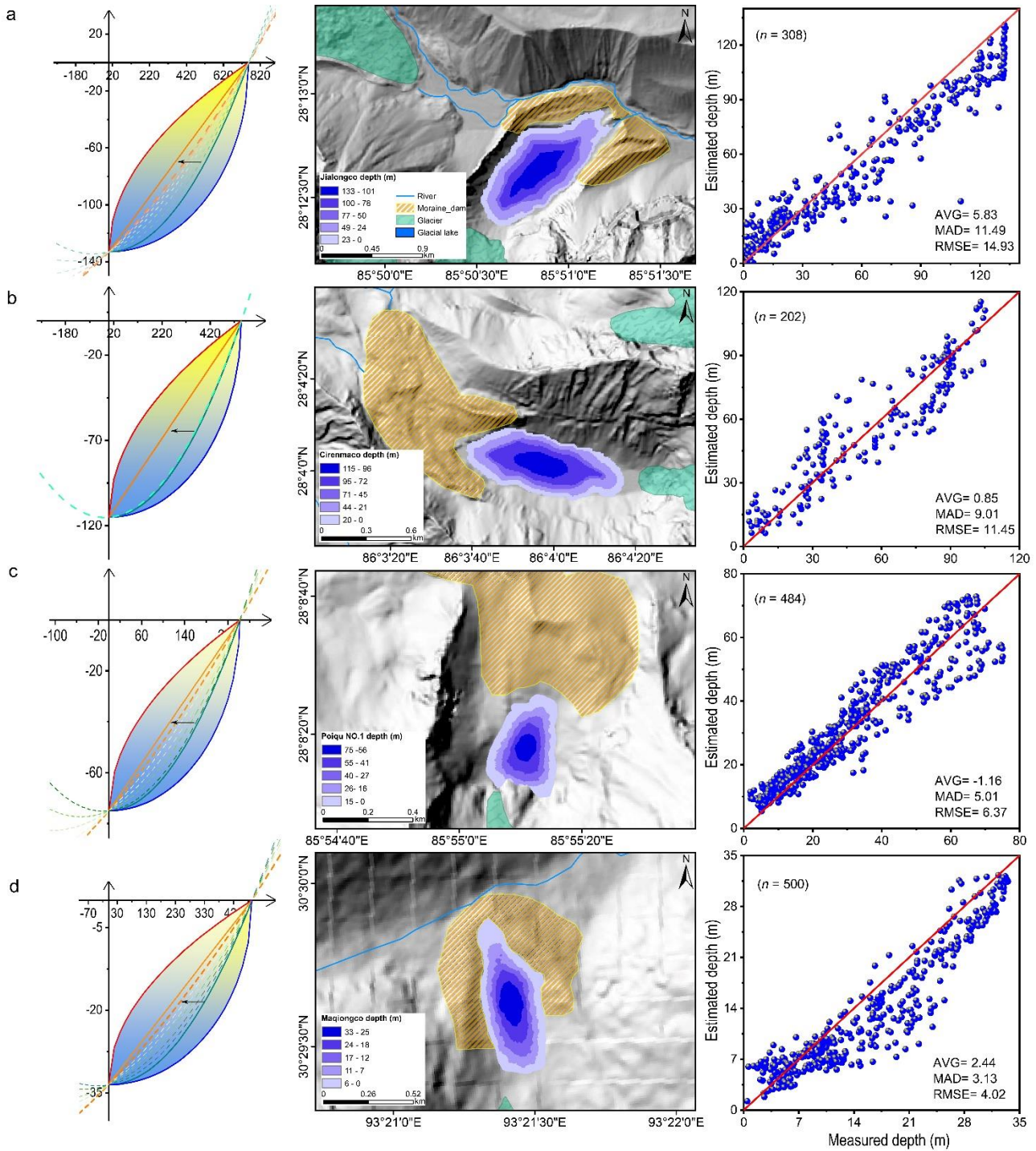
### 242 **3 Results**

243 We present the SCMs for each type of glacial lake and demonstrate a procedure to identify the most compatible  
244 GCM for a specific glacial lake by equalizing the volume of both. To our knowledge, this is the first model to simulate  
245 the bathymetric distribution of glacial lakes at present. The results reveal that the proglacial and periglacial lakes  
246 exhibit greater depths as their SCMs are closer to the hemisphere structured by the upward-opening parabolic side.  
247 Conversely, the SCMs of the extraglacial and supraglacial lakes are closer to the cone structured by the straight side,  
248 indicating relatively shallower depths. As the ice-dammed lake, their V–A fitting curve is more similar to the V–A  
249 curve of the triangular cone (Fig. 4). Hence, we recommend that the bathymetric distribution modeling for ice-  
250 dammed lakes proceeds directly using the standard triangular cone.

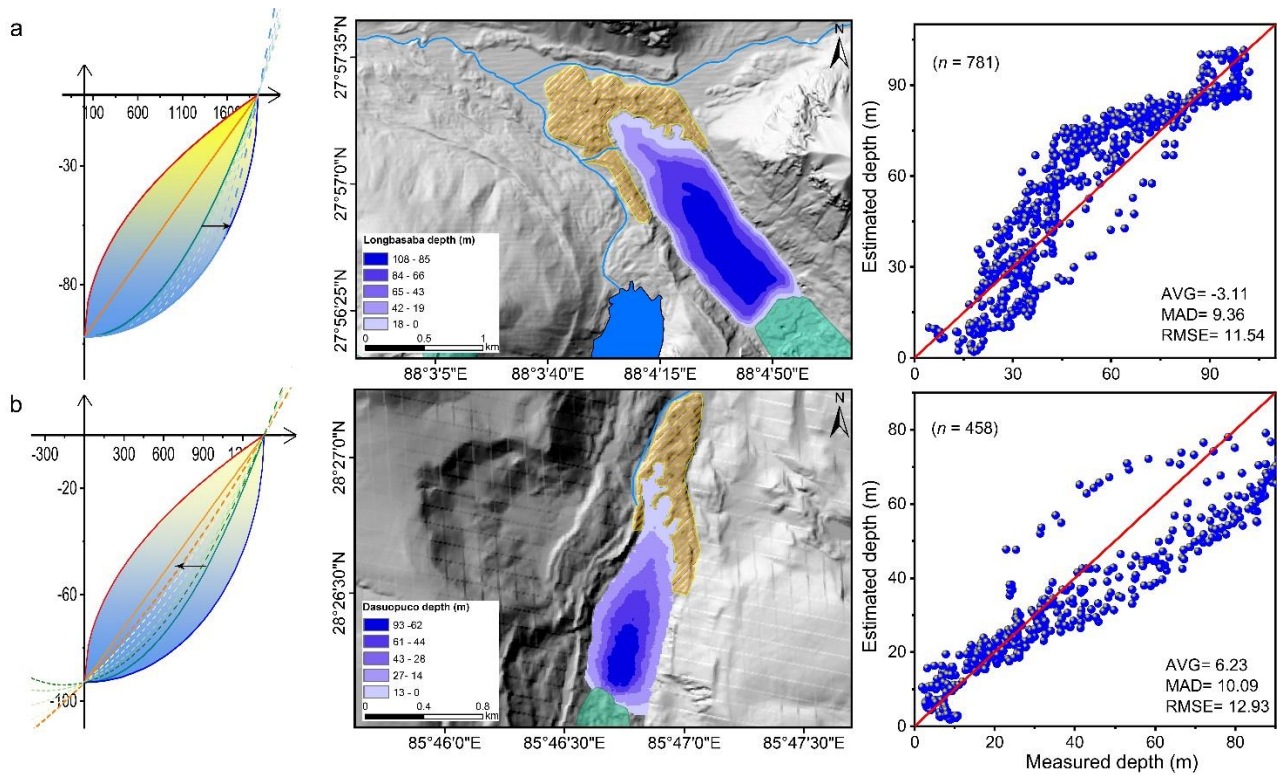
251 We determined the optimal GCMs for the six exhibited glacial lakes. Following bathymetric distribution  
252 modeling results, the total volume of Jialongco was calculated to be  $33.1 \times 10^6 \text{ m}^3$  (with a relative error of  $-11.7\%$ )  
253 with a mean water depth of  $54.6 \text{ m}$  ( $-8.1\%$ ). Its GCM was closer to the cone structured by the straight side (Fig. 7a).  
254 The computed total volume and mean depth of Cirenmaco were  $17.2 \times 10^6 \text{ m}^3$  ( $-4.4\%$ ) and  $51.7 \text{ m}$  ( $-6.9\%$ ),  
255 respectively. The Cirenmaco GCM had similarities with the hemisphere structured by the upward-opening parabolic  
256 side (Fig. 7b), meaning a more significant inward deepening rate than Jialongco. The relatively small-sized Poiqu  
257 NO.1 and Maqiongco had total volumes of  $2.9 \times 10^6 \text{ m}^3$  ( $7.4\%$ ) and  $3 \times 10^6 \text{ m}^3$  ( $-6.3\%$ ), and mean water depths of  $27.3$   
258  $\text{m}$  ( $7.1\%$ ) and  $12.8 \text{ m}$  ( $-14.7\%$ ), respectively. Their optimal GCMs showed similarities with Jialongco (Fig. 7c, d).  
259 The proglacial lake, Longbasaba, was estimated to have a total volume of  $71.4 \times 10^6 \text{ m}^3$  ( $11.5\%$ ) and a mean depth of  
260  $61.1 \text{ m}$  ( $22.2\%$ ). Its GCM was more resemblant to the semi-ellipsoid (Fig. 8a). Dasuopuco had the smallest relative  
261 error in the total volume ( $0.2\%$ ) and mean water depth ( $-1.8\%$ ) (Fig. 8b). Overall, approximately  $\pm 10\%$  volume  
262 uncertainty was estimated in the process of nesting the general conceptual models to the actual glacial lake shapes.

263 The disparity between the area of the assumed standard ellipse surface and the actual lake surface, as well as the  
264 deviation of the deepest water location, likely caused the majority of the inaccuracy. The initial settings of glacial  
265 lake conceptual models and the algorithm's applicability were confirmed by comparison with the measured and  
266 estimated individual water depths. Between the estimated and measured water depths along the bathymetric routes,  
267 the average deviation, mean absolute deviation, and root mean square error for the six glacial lakes all described good

268 consistency. Neither near the lakeshore nor the lake center do the estimates show intolerable dispersions.



269  
 270 **Figure 7.** Modeled glacial lake bathymetric distributions of the four selected periglacial lakes. (a) Jialongco, (b) Cirenmaco, (c) Poiqu  
 271 NO.1, and (d) Maqiongco. The average deviation (AVG), mean absolute deviation (MAD), and root mean square error (RMSE) were  
 272 selected to depict the consistency between the simulated and measured individual water depths along the boat routes. The movements  
 273 of the general curves from one standard curve to another are also indicated.



274

275 **Figure 8.** Modeled glacial lake bathymetric distributions of the two selected proglacial lakes. (a) Longbasaba Lake, and (b) Dasuopuco.  
 276 The average deviation (AVG), mean absolute deviation (MAD), and root mean square error (RMSE) were selected to depict the  
 277 consistency between the simulated and measured individual water depths along the boat routes. The movements of the general curves  
 278 from one standard curve to another are also indicated.

279

## 280 4 Discussion

### 281 4.1 Glacial lake basin evolution

282 Understanding the glacial lake evolution can help comprehend these idealized geometric shapes in theory. Most  
 283 moraine- or bedrock-dammed lakes develop in depressions exposed by diminishing glaciers. The supraglacial lakes  
 284 exist at the glacier snout, eventually facilitating the formation of proglacial and periglacial lakes (Carrivick and Tweed,  
 285 2013). As the six glacial lakes illustrated, our hypotheses explained the different rates of inward deepening owing to  
 286 the influence of exogenous materials. The glacier bedrock has been eroded and nudged during historical ice flowing,  
 287 posing the excavation and growth of glacial lake basins.

288 Contemporary glaciers often have a certain thickness of debris at the snout. For example, approximately 1 m of  
 289 debris was observed at the snout of the Urumqi Glacier No. 1, China (Echelmeyer et al., 1987) as the result of glacial



290 erosion. The specific sites of continual eroding and nudging spawn overdeepenings and are considered potential  
291 glacial lakes (Linsbauer et al., 2016). Since the glacier velocity in the middle part is often larger than that of both  
292 sides, the erosion is stronger in the central line of the initial overdeepening. As glacier flowing continues, the shape  
293 of the overdeepening finally reaches equilibrium and is similar to a hemisphere, which is the GCM of the lake basin  
294 we assumed. After the overdeepenings are exposed, they can be filled by meltwater to form glacial lakes while also  
295 receiving material deposition, resulting in a gradual transition of the idealized geometric basin from a hemisphere to  
296 a cone. This conjecture can be inferred from the studies of overdeepenings on glacial beds, whereby the volume and  
297 surface area of these potential glacial lakes are also in accordance with the power-law relationship (Zhang et al.,  
298 2022).

## 299 **4.2 Applicability of the conceptual model**

300 Our modeling theory is based on the observations of glacial lake bathymetric distribution characteristics  
301 worldwide, revealing a universal geometrical approximation law for glacial lake bathymetry. Therefore, this  
302 modeling approach may be applicable to most glacial lakes in mountain glaciers. However, it is strictly limited by  
303 several constraints. Firstly, the designed conceptual model is more suitable for those glacial lakes with typically  
304 lengthy and elliptical-like shapes, and may be less applicable to very irregularly shaped glacial lakes, such as the ice-  
305 marginal and thermokarst lakes in the Greenland and Alaska region (Field et al., 2021; Coulombe et al., 2022).  
306 Similarly, we did not collect any glacial lake bathymetry data in polar regions which causes non-applicability on  
307 supraglacial lakes over the Greenland/Antarctic Ice sheets. Secondly, the parent glaciers of glacial lakes can be a  
308 cirque-valley glacier or a small/medium sized valley glacier flowing along a straight valley, ensuring idealized  
309 formation conditions for the glacial lake basin with minimal erosion and deposition from tributaries.

310 Although the simulated results were only validated in the periglacial and proglacial lakes of the Himalayas  
311 and Nyainqentanglha due to limited observation data, the comparison results of the measured and modeled depth  
312 values at different locations of the six glacial lakes demonstrates the rationality and reliability of our conceptual  
313 models. In addition to the subjective and objective errors made during the modeling phase, there are several  
314 systematic defects in the algorithm itself: (1) The total volume and maximum water depth are calculated using  
315 empirical equations, which may lead to significant deviations when modeling the bathymetric distribution of an  
316 arbitrarily selected glacial lake. Particularly, the curves of D–A are not robust, with many discrete points appearing  
317 (Fig. 2). (2) The estimated depth contours converge inward using the lake shoreline buffers first, followed by the

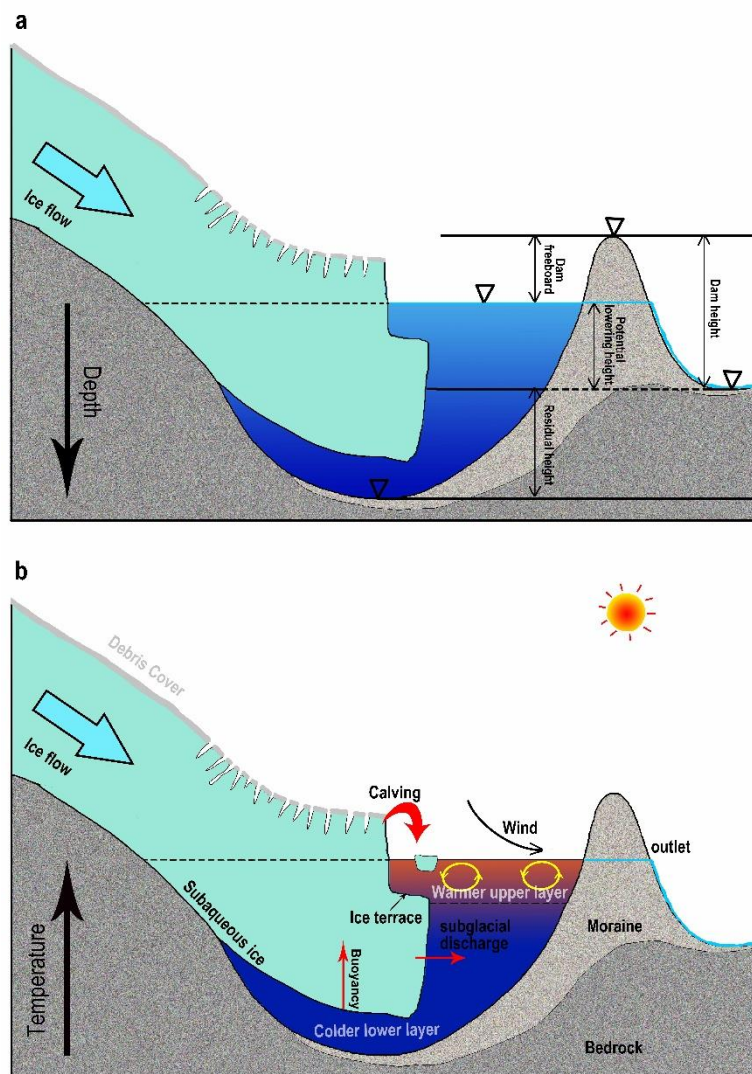
318 elliptical surfaces. This process may effectively simulate the connections between a bathymetric distribution and  
319 glacial lake morphology. However, it is not essential. If the elliptical indentations are always inward relative to the  
320 elliptical surface, the modeling accuracy is also not affected significantly in theory. (3) The deepest sites of proglacial  
321 lakes have been considered to be near the glacier-lake interface. The developing proglacial lakes, however, are  
322 complex. Their deepest sites are constantly located near the glacier terminus before the deepest site of overdeepening  
323 is exposed (Fig. 9a), which is in accordance with our hypothesis. With the deepest sites developing more fully, they  
324 gradually shift toward the lake center. Our algorithm has not addressed these changes. In the future, the conceptual  
325 model will require parameter optimization through learning with a number of measured bathymetry data. Furthermore,  
326 the present version of our algorithm relies on simple programming and semi-automated geospatial analysis tools  
327 processing. We will further develop this conceptual model to create an interface that can automatically process and  
328 reduce subjective errors.

### 329 **4.3 Rationality of empirical V-A equations**

330 Currently, many studies have attempted to fit V-A equations with regional or global applicability for various  
331 types of glacial lakes (Cook et al., 2015; Qi et al., 2022). The most common classification method for glacial lakes is  
332 based on dam materials, such as moraine-dammed, bedrock-dammed, and landslide-dammed. However, this study  
333 reveals that the different types of glacial lakes have different ideal basin shapes that may be unfavorable to most  
334 already formed V-A empirical formulations, although some have high  $R^2$  values (Table 1). For instance, most of the  
335 proglacial and periglacial lakes is generally dammed by moraine, involving in many fitting works of V-A relationships.  
336 Unreasonably, the incompletely developed basins of proglacial lakes and the fully developed basins of periglacial  
337 lakes are often described by same empirical formulas (Fig. 9a), disregarding the distinct basin development stages  
338 between them. This aspect has overlooked in the previous studies. In our fitted curves of V-A relationships for various  
339 types of glacial lakes (Fig. 4), the V-A relationship for proglacial lakes is robust, indicating possible global  
340 applicability. However, the V-A relationships for periglacial and extraglacial lakes exhibit many outliers, suggesting  
341 a strong influence from exogenous materials filling in these lakes based on our hypothesis. The V-A relationships of  
342 these glacial lakes decoupled with their glaciers at least require parameters related to the glacier characteristics and  
343 time of detachment for further description.

344 There is no single classification method can adequately capture the refined characteristics of glacial lakes. Even  
345 lakes classified as the same type may differ in terms of parent glaciers, bedrock properties, or dam materials. In the

346 modeling of glacial lake bathymetric distribution, accurately estimating the total volume and maximum water depth  
 347 of glacial lakes is crucial. Therefore, future studies should not only focus on whether the empirical formula is  
 348 generalizability or global applicability, but also develop more detailed classification criteria for glacial lakes,  
 349 comprehensively considering dam materials, topological positions, glacier properties, area intervals, geographic  
 350 location, and other relevant factors. This will facilitate a well-fitting of regional empirical relationships of V-A and  
 351 D-A for various types of glacial lakes, thereby reducing the dispersion between data points.



352  
 353 **Figure 9.** The schematic diagrams illustrate (a) the potential maximum lowering height of the glacial lake water level after drainage and  
 354 (b) the interactions between the parent glacier and its terminating lake.

#### 355 4.4 Applications in GLOF modeling

356 The applicability of a glacial lake bathymetric distribution has been addressed in this study; one such application

357 is in GLOF modeling. The results make two significant contributions to future GLOF modeling: (i) accurately  
358 estimate the maximum potential outburst water volume of a glacial lake by combining lake surface elevation, dam  
359 bottom elevation, and the optimal GCM; (ii) facilitate coupling between the various GLOF processes in modeling  
360 (trigger–displacement wave–dam breach–flood propagation). Many recent studies have documented reconstructing  
361 the historical GLOFs and simulating the future GLOFs from high outburst potential glacial lakes (Allen et al., 2015;  
362 Anaconda et al., 2015b; Erokhin et al., 2017; Kougkoulos et al., 2018). The modeling precision is expected to improve  
363 significantly.

364 On the one hand, most prior studies replaced the potential maximum outburst volume with the total water volume  
365 because of the limitations of glacial lake bathymetric investigations (Zhang et al., 2021). Although this could present  
366 a maximized risk assessment, an inflated downstream exposure might raise excessive concerns among the authorities  
367 and the public regarding inadequate prevention and mitigation measures (Emmer et al., 2022b). As long as the dam’s  
368 lowest elevation exceeds that of the glacial lake (potential lowering height is less than the maximum water depth), it  
369 could result in incomplete drainage (Fig. 9a). On the other hand, due to the complicated phase transition in the chain  
370 process of GLOFs, a segmented simulation has been generally conducted. For instance, Rapid Mass Movement  
371 Simulation (RAMMS) can be used to simulate the impact of ice avalanches or landslides on glacial lakes (Frey et al.  
372 2018; Sattar et al. 2021), and hydrological algorithms are used to calculate the displacement wave (Heller et al. 2009;  
373 Evers et al. 2019). Modeling software like IBER, HEC-RAS, or FLO-2D are employed to simulate downstream flood  
374 propagation (Alho and Aaltonen, 2008; Osti and Egashira, 2009; Schneider et al., 2014; Somos-Valenzuela et al.,  
375 2015; Maurer et al., 2020; Nie et al. 2020).

376 In contrast to a holistic simulation, such a segmented simulation approach undoubtedly causes poor articulation  
377 and increased uncertainty in different processes. With the recent scientific developments, a newly developed three-  
378 phase flow model, r.avaflow (Mergili et al., 2017), started to be used to simulate GLOF propagations (Mergili et al.,  
379 2018, 2020) and can realize the whole hazard cascade modeling with a high performance (Zheng et al., 2021). Our  
380 study can provide much-needed glacial lake bathymetry data for such modeling to calculate the displacement wave  
381 in the lake surface and the water release process during dam erosion.

#### 382 **4.5 Potential developments of numerical or physical models**

383 The standardized glacial lake basin can facilitate other future model development related to glacial lakes and  
384 improve knowledge of how the proglacial lakes and lake-terminating glaciers interact. Carrivick et al. (2020)

385 discussed six major challenges in constructing a numerical model of interactions between proglacial lakes and  
386 glaciers, which include the imperative for glacial lake bathymetry. The standardized shape implicates the design of  
387 the model's basic architecture.

388 Compared with the somewhat realistic glacier bed topography within the overdeepenings revealed by Ice  
389 Thickness Models, a standardized lake basin provides an alternative scheme. For a specific proglacial lake, its water  
390 level, water temperature, in/outflow, internal circulation, and interface with the glacier vary with glacier-lake  
391 dynamics and time, which are very complex processes (Sugiyama et al., 2016; Sutherland et al., 2020). Deep and  
392 large proglacial lakes are prone to water stratification due to warmer upper layers and colder lower layers of water  
393 because these freshwater terminating lakes currently have no evidence of active internal circulation (Haresign and  
394 Warren, 2005; Boyce et al., 2007). This stratification induces the subaqueous ice differential melting and ice terrace  
395 formation (Fig. 9b), impacting the glacier terminal calving regimes (Sugiyama et al., 2019; Mallalieu et al., 2020).  
396 On the other hand, the dynamic characteristics of glacier snout, such as bed friction, longitudinal stress, and ice flow  
397 velocity, vary distinctively due to the presence of terminating lakes (Sugiyama et al., 2011; Liu et al., 2020). The  
398 knowledge and understanding of glacial lakes formation and evolution changes continually. The ultimate goal is to  
399 present these processes via computer numerical simulations. Yet, the idealized lake basin can facilitate calculating  
400 the mass and energy transport at the interface.

401

## 402 **5 Conclusion**

403 This study was conducted in response to a circumstance that field investigation was the only approach to obtain  
404 glacial lake bathymetry. The relationships of volume–area and maximum water depth–area of glacial lakes were  
405 reanalyzed via an inventory of the global glacial lake bathymetry data we compiled. The obtained curves were  
406 matched with a power-law relationship. Thus, the types of hemispheres or cones were determined as the conceptual  
407 models (idealized geometric shapes) of glacial lakes. The standard lake surface was assumed to be an ellipse.

408 Nine standard conceptual models were identified. The SCMs for the supraglacial, periglacial, and extraglacial  
409 lakes are the hemisphere structured by the elliptical side; the hemisphere structured by the upward-opening parabolic  
410 side; the cone structured by the straight side; and the cone structured by the rightward-opening parabolic side. The  
411 SCMs for the proglacial lakes were determined to be half of the aforementioned four SCMs. Two SCMs were  
412 considered for the ice-dammed lakes: the semi–cone structured by the straight side and the triangular cone. To depict

413 the volume between the two SCMs, a general conceptual model was defined to represent the transition from one  
414 SCM to another.

415 Several hypotheses are important in our algorithm to nest the actual glacial lake shapes from idealized  
416 conceptual models and interpolate glacial lake bathymetric distribution. First, the supraglacial, periglacial, and  
417 extraglacial lakes' deepest sites were assumed to be in the lake center, whereas the proglacial lakes and ice-dammed  
418 lakes' deepest sites were near the glacier-lake interface. Second, the effects of exogenous materials and boundary  
419 conditions were used to explain the different rates of inward deepening of glacial lakes. Six glacial lakes with  
420 measured bathymetry data were selected in the Third Pole region for comparison with the simulated bathymetric  
421 distributions. The results demonstrated good accuracy and applicability of our conceptual models in estimating lake  
422 bathymetry. Relatively high consistency was shown in the point-to-point comparisons of the measured and simulated  
423 water depths. This study constructed the glacial lake bathymetric distribution model which is very rewarding for  
424 comprehending the evolution of glacial lakes. Moreover, the quality of GLOF modeling and risk assessment is also  
425 enhanced by our outlined general conceptual model. These standardized lake basins implicate the design of the  
426 model's basic architecture, which can potentially promote the development of future numerical or physical models  
427 of glacial lakes.

428

429 *Code availability.* The codes for calculating the functional equations of a general conceptual model in the coordinate  
430 axes are available on request.

431 *Data availability.* The observed bathymetric data of Jialongco and Longbasaba Lake were provided by Dr. Xiaojun  
432 Yao and Donghui Shangguan, respectively. The observed bathymetric data of Poiqu NO.1, Dasuopuco, and  
433 Maqiongco can be freely downloaded at <https://doi.org/10.6084/m9.figshare.21569175> (Zhang et al., 2023).

434 *Supplement.* The supplement related to this article is available online at: <https://tc.copernicus.org/preprints/tc-2023-12/tc-2023-12-supplement.zip>.

436 *Author contributions.* TZ and WW designed the study, compiled the data and drafted the manuscript. BA revised and  
437 edited the manuscript.

438 *Competing interests.* The authors declare that they have no conflict of interest.

439 *Acknowledgements.* We thank the two anonymous reviewers, Dr. Adam Emmer and the editor, Xichen Li, for the  
440 constructive comments that improved the paper.

441 *Financial support.* This study was supported by the Second Tibetan Plateau Scientific Expedition and Research  
442 (STEP) Program (2019QZKK0208); the Strategic Priority Research Program of the Chinese Academy of Sciences  
443 (XDA20100300); and the International Partnership Program of Chinese Academy of Sciences  
444 (131C11KYSB20200029).

445

## 446 **References**

- 447 Aggarwal, S., Rai, S. C., Thakur, P. K., and Emmer, A.: Inventory and recently increasing GLOF susceptibility of glacial lakes in Sikkim,  
448 Eastern Himalaya, *Geomorphology*, 295, 39–54, <http://dx.doi.org/10.1016/j.geomorph.2017.06.014>, 2017.
- 449 Alho, P., and Aaltonen, J.: Comparing a 1D hydraulic model with a 2D hydraulic model for the simulation of extreme glacial outburst  
450 floods, *Hydrol. Process*, 22, 1537–1547. <http://dx.doi.org/10.1002/hyp.6692>, 2018.
- 451 Allen, S. K., Rastner, P., Arora, M., Huggel, C., and Stoffel, M. (2016). Lake outburst and debris flow disaster at Kedarnath, June 2013:  
452 hydrometeorological triggering and topographic predisposition, *Landslides*, 13, 1479–1491, [http://dx.doi.org/10.1007/s10346-015-](http://dx.doi.org/10.1007/s10346-015-0584-3)  
453 0584-3, 2015.
- 454 Anaconda, P. I., Mackintosh, A., Norton, K. P.: Hazardous processes and events from glacier and permafrost areas: lessons from the  
455 Chilean and Argentinean Andes, *Earth Surf. Process Landf.*, 40, 2–21, <http://dx.doi.org/10.1002/esp.3524>, 2015a.
- 456 Anaconda, P. I., Mackintosh, A., Norton, K.: Reconstruction of a glacial lake outburst flood (GLOF) in the Engano Valley, Chilean  
457 Patagonia: Lessons for GLOF risk management, *Sci. Total Environ.*, 527–528, 1–11,  
458 <http://dx.doi.org/10.1016/j.scitotenv.2015.04.096>, 2015b.
- 459 Bolch, T., Buchroithner, M. F., Peters, J., Pradhan, B., Buchroithner, M., and Blagoveshchensky, V.: Identification of glacier motion and  
460 potentially dangerous glacial lakes in the mt. Everest region/Nepal using spaceborne imagery, *Nat. Hazard Earth Syst.*, 8, 1329–  
461 1340, <http://dx.doi.org/10.1007/s11069-011-9860-2>, 2011.
- 462 Boyce, E. S., Motyka, R. J., and Truffer, M.: Flotation and retreat of a lake-calving terminus, Mendenhall Glacier, southeast Alaska,  
463 USA, *J. of Glaciol.*, 53, 211–224, <http://dx.doi.org/10.3189/172756507782202928>, 2007.
- 464 Carrivick, J. L., and Tweed, F. S.: Proglacial lakes: character, behaviour and geological importance, *Quat. Sci. Rev.*, 78, 34–52,  
465 <http://dx.doi.org/10.1016/j.quascirev.2013.07.028>, 2013.
- 466 Carrivick, J. L., and Tweed, F. S.: A global assessment of the societal impacts of glacier outburst floods, *Glob. Planet. Change*, 144, 1–  
467 16, <http://dx.doi.org/10.1016/j.gloplacha.2016.07.001>, 2016.
- 468 Carrivick, J. L., Tweed, F. S., Sutherland, J. L., and Mallalieu, J.: Toward numerical modeling of interactions between ice-marginal  
469 proglacial lakes and glaciers, *Front. Earth Sci.*, 500, <https://doi.org/10.3389/feart.2020.577068>, 2020.
- 470 Cook, S. J., Quincey, D. J.: Estimating the volume of Alpine glacial lakes, *Earth Surf. Dyn.*, 3, 559–575, [http://www.earth-surf-](http://www.earth-surf-dynam.net/3/559/2015/doi:10.5194/esurf-3-559-2015)  
471 [dynam.net/3/559/2015/doi:10.5194/esurf-3-559-2015](http://www.earth-surf-dynam.net/3/559/2015/doi:10.5194/esurf-3-559-2015), 2015.
- 472 Coulombe, S., Fortier, D., Bouchard, F., Paquette, M., Charbonneau, S., Lacelle, D., Laurion, I. and Pienitz, R. Contrasted  
473 geomorphological and limnological properties of thermokarst lakes formed in buried glacier ice and ice-wedge polygon terrain,  
474 *Cryosphere*, 16, 2837–2857. <https://doi.org/10.5194/tc-16-2837-2022>, 2022.
- 475 Drenkhan, F., Huggel, C., Guardamino, L., and Haeblerli, W.: Managing risks and future options from new lakes in the deglaciating  
476 Andes of Peru: The example of the Vilcanota-Urubamba basin, *Sci. Total Environ.*, 665, 465–483,



477 <https://doi.org/10.1016/j.scitotenv.2019.02.070>, 2019.

478 Echelmeyer, K., Wang Z. X.: Direct observation of basal sliding and deformation of basal drift at sub-freezing temperatures, *J. Glaciol.*,  
479 33, 83–98. <http://dx.doi.org/10.3189/s0022143000005396>, 1987.

480 Emmer, A., and Vilímek, V.: New method for assessing the susceptibility of glacial lakes to outburst floods in the Cordillera Blanca,  
481 Peru, *Hydrol. Earth Syst. Sci.*, 18, 3461–3479, <http://www.hydrol-earth-syst-sci.net/18/3461/2014/doi:10.5194/hess-18-3461-2014>,  
482 2014.

483 Emmer, A., Klimeš, J., Mergili, M., Vilímek, V. and Cochachin, A.: 882 lakes of the Cordillera Blanca: An inventory, classification,  
484 evolution and assessment of susceptibility to outburst floods, *Catena*, 147, 269–279, <http://dx.doi.org/10.1016/j.catena.2016.07.032>,  
485 2016.

486 Emmer, A., Allen, S.K., Carey, M., Frey, H., Huggel, C., Korup, O., Mergili, M., Sattar, A., Veh, G., Chen, T.Y., Cook, S.J., Correas-  
487 Gonzalez, M., Das, S., Diaz Moreno, A., Drenkhan, F., Fischer, M., Immerzeel, W.W., Izagirre, E., Joshi, R.C., Koukoulos, I.,  
488 Kuyakanon Knapp, R., Li, D., Majeed, U., Matti, S., Moulton, H., Nick, F., Piroton, V., Rashid, I., Reza, M., Ribeiro de Figueiredo,  
489 A., Riveros, C., Shrestha, F., Shrestha, M., Steiner, J., Walker-Crawford, N., Wood, J.L. and Yde, J.C. Progress and challenges in  
490 glacial lake outburst flood research (2017–2021): a research community perspective, *Nat. Hazard Earth Syst. Sci.*, 22, 3041–3061.  
491 <https://doi.org/10.5194/nhess-22-3041-2022>, 2022a.

492 Emmer, A., Wood, J.L., Cook, S.J., Harrison, S., Wilson, R., Diaz-Moreno, A., Reynolds, J.M., Torres, J.C., Yarleque, C., Mergili, M.,  
493 Jara, H.W., Bennett, G., Caballero, A., Glasser, N.F., Melgarejo, E., Riveros, C., Shannon, S., Turpo, E., Tinoco, T., Torres, L.,  
494 Garay, D., Villafane, H., Garrido, H., Martinez, C., Apaza, N., Araujo, J. and Poma, C. 160 glacial lake outburst floods (GLOFs)  
495 across the Tropical Andes since the Little Ice Age, *Global Plane. Change*, 208. <https://doi.org/10.1016/j.gloplacha.2021.103722>,  
496 2022b.

497 Erokhin, S. A., Zaginaev, V. V., Meleshko, A. A., Ruiz-Villanueva, V., Petrakov, D. A., Chernomorets, S. S., Viskhadzhieva, K. S.,  
498 Tutubalina, O. V., and Stoffel, M.: Debris flows triggered from non-stationary glacier lake outbursts: the case of the Teztor Lake  
499 complex (Northern Tian Shan, Kyrgyzstan), *Landslides*, 15, 83–98, <http://dx.doi.org/10.1007/s10346-017-0862-3>, 2018.

500 Evans, S. G.: The maximum discharge of outburst floods caused by the breaching of man-made and natural dams, *Can. Geotech. J.*,  
501 23(3), 385–387, <http://dx.doi.org/10.1139/t87-062>, 1986.

502 Evers F. M., Heller, V., Fuchs, H., Hager, W. H., and Boes, R. M.: Landslide-generated Impulse Waves in Reservoirs: Basics and  
503 Computation, *VAW-Mitteilungen*, 254, 2019.

504 Falatkova, K., Šobr, M., Neureiter, A., Schöner, W., Janský, B., Häusler, H., Engel, Z., and Beneš, V.: Development of proglacial lakes  
505 and evaluation of related outburst susceptibility at the Adygin ice-debris complex, northern Tien Shan, *Earth Surf. Dyn.*, 7, 301–  
506 320, <https://doi.org/10.5194/esurf-7-301-2019>, 2019.

507 Field, H.R., Armstrong, W.H. and Huss, M. Gulf of Alaska ice-marginal lake area change over the Landsat record and potential physical  
508 controls, *Cryosphere*, 15, 3255–3278. <https://doi.org/10.5194/tc-15-3255-2021>, 2021.

509 Frey, H., Huggel, C., Chisolm, R. E., Baer, P., McArdeell, B., Cochachin, A., and Portocarrero, C.: Multi-source glacial lake outburst  
510 flood hazard assessment and mapping for Huaraz, Cordillera Blanca, Peru, *Front. Earth Sci.*, 6, 210.  
511 <https://doi.org/10.3389/feart.2018.00210>, 2018.

512 Fujita, K., Sakai, A., Takenaka, S., Nuimura, T., Surazakov, A. B., Sawagaki, T., and Yamanokuchi, T.: Potential flood volume of  
513 Himalayan glacial lakes, *Nat. Hazard Earth Syst. Sci.*, 13, 1827–1839, [http://www.nat-hazards-earth-syst-  
514 sci.net/13/1827/2013/doi:10.5194/nhess-13-1827-2013](http://www.nat-hazards-earth-syst-sci.net/13/1827/2013/doi:10.5194/nhess-13-1827-2013), 2013.

515 Haresign, E., and Warren, C. R.: Melt rates at calving termini: a study at Glaciar León, Chilean Patagonia, Geological Society, London,  
516 *Special Publications*, 242, 99–109, <http://dx.doi.org/10.1144/GSL.SP.2005.242.01.09>, 2005.

517 Heller, V., Hager, W. H., Minor, H. E.: *Landslide Generated Impulse Waves in Reservoirs*, Zurich: Mitteilungen Versuchsanstalt für  
518 Wasserbau, Hydrologie und Glaziologie (VAW), ETH Zürich, 2019.

519 Huggel, C., Kääh, A., Haerberli, W., Haerberli, W., Teysseire, P., and Paul, F.: Remote sensing based assessment of hazards from glacier  
520 lake outbursts: a case study in the Swiss Alps, *Can. Geotech. J.*, 39, 316–330, <http://dx.doi.org/10.1139/t01-099>, 2002.

521 Hugonnet, R., McNabb, R., Berthier, E., Menounos, B., Nuth, C., Girod, L., Farinotti, D., Huss, M., Dussailant, I., Brun, F., and Kääh,  
522 A.: Accelerated global glacier mass loss in the early twenty-first century, *Nature*, 592, 726–731, [https://doi.org/10.1038/s41586-](https://doi.org/10.1038/s41586-021-03436-z)  
523 021-03436-z, 2021.

524 Kapitsa, V., Shahgedanova, M., Machguth, H., Severskiy, I., and Medeu, A.: Assessment of evolution and risks of glacier lake outbursts  
525 in the Djungarskiy Alatau, Central Asia, using Landsat imagery and glacier bed topography modelling, *Nat. Hazard Earth Syst. Sci.*,  
526 17, 1837–1856, <https://doi.org/10.5194/nhess-17-1837-2017>, 2017.

527 Khanal, N. R., Hu, J. M., and Mool, P.: Glacial lake outburst flood risk in the Poiqu/Bhote Koshi/Sun Koshi river basin in the Central  
528 Himalayas, *Mt. Res. Dev.*, 35, 351–364, <http://dx.doi.org/10.1659/MRD-JOURNAL-D-15-00009>, 2015.

529 Kougkoulos, I., Cook, S. J., Edwards, L. A., Clarke, L. J., Symeonakis, E., Dortch, J. M., and Nesbitt, K.: Modelling glacial lake outburst  
530 flood impacts in the Bolivian Andes, *Nat. Hazard*, 94, 1415–1438, <https://doi.org/10.1007/s11069-018-3486-6>, 2018.

531 Li, D., Shangguan, D. H., Wang, X., Ding, Y. J., Su, P. C., Liu, R. L., and Wang, M. X.: Expansion and hazard risk assessment of glacial  
532 lake Jialong Co in the central Himalayas by using an unmanned surface vessel and remote sensing, *Sci. Total Environ.*, 784,  
533 <https://doi.org/10.1016/j.scitotenv.2021.147249>, 2021.

534 Linsbauer, A., Frey, H., Haeberli, W., Machguth, H., Azam, M. F., and Allen, S.: Modelling glacier-bed overdeepenings and possible  
535 future lakes for the glaciers in the Himalaya—Karakoram region, *Ann. Glaciol.*, 57, 119–130,  
536 <http://dx.doi.org/10.3189/2016AoG71A627>, 2016.

537 Liu, Q., Mayer, C., Wang, X., Nie, Y., Wu, K. P., Wei, J. F., and Liu, S. Y.: Interannual flow dynamics driven by frontal retreat of a lake-  
538 terminating glacier in the Chinese Central Himalaya, *Earth Planet. Sci. Lett.*, 546, 116450,  
539 <https://doi.org/10.1016/j.epsl.2020.116450>, 2020.

540 Lliboutry, L., Arnao, B. M., Pautre, A., and Schneider, B.: Glaciological problems set by the control of dangerous lakes in Cordillera  
541 Blanca, Peru. I. Historical failures of morainic dams, their causes and prevention, *J. Glaciol.*, 18, 239–254,  
542 <http://dx.doi.org/10.1017/S002214300002133X>, 1977.

543 Loriaux, T., Casassa, G.: Evolution of glacial lakes from the Northern Patagonia Icefield and terrestrial water storage in a sea-level rise  
544 context, *Glob. Planet. Change*, 102, 33–40, <http://dx.doi.org/10.1016/j.gloplacha.2012.12.012>, 2013.

545 Lützwow, N., Veh, G. and Korup, O. A global database of historic glacier lake outburst floods, *Earth Sys. Sci. Data*, (in discussion).  
546 <http://dx.doi.org/10.5194/essd-2022-449>, 2023.

547 Ma, J. S., Song, C. Q., Wang, Y. J.: Spatially and Temporally Resolved Monitoring of Glacial Lake Changes in Alps During the Recent  
548 Two Decades, *Front. Earth Sci.*, 9, <https://doi.org/10.3389/feart.2021.723386>, 2021.

549 Mallalieu, J., Carrivick, J. L., Quincey, D. J., and Smith, M. W.: Calving seasonality associated with melt-undercutting and lake ice  
550 cover, *Geophys. Res. Lett.*, 47, e2019GL086561, <https://doi.org/10.1029/2019GL086561>, 2020.

551 Maurer, J. M., Schaefer, J. M., Russell, J. B., Rupper, S., Wangdi, N., Putnam, A. E., and Young, N.: Seismic observations, numerical  
552 modeling, and geomorphic analysis of a glacier lake outburst flood in the Himalayas, *Sci. Adv.*, 6, eaba3645,  
553 <http://dx.doi.org/10.1126/sciadv.aba3645>, 2020.

554 Mergili, M., Fischer, J. T., Krenn, J., Pudasaini, S. P.: r. avaflow v1, an advanced open-source computational framework for the  
555 propagation and interaction of two-phase mass flows, *Geosci. Model Develop.*, 10, 553–569, [http://dx.doi.org/10.5194/gmd-10-](http://dx.doi.org/10.5194/gmd-10-553-2017)  
556 553-2017, 2017.

557 Mergili, M., Emmer, A., Juricova, A., Cochachin, A., Fischer, G. T., Huggel, C., and Pudasaini, S. P.: How well can we simulate complex  
558 hydro-geomorphic process chains? The 2012 multi-lake outburst flood in the Santa Cruz Valley (Cordillera Blanca, Peru), *Earth*  
559 *Surf. Process. Landf.*, 431373–1389, <http://dx.doi.org/10.1002/esp.4318>, 2018.

560 Mergili M, Pudasaini SP, Emmer A, Fischer, G. T., Cochachin, A., Frey, H.: Reconstruction of the 1941 GLOF process chain at Lake  
561 Palcacocha (Cordillera Blanca, Peru), *Hydrol. Earth Syst. Sci.*, 24, 93–114, <https://doi.org/10.5194/hess-24-93-2020>, 2020.

562 Miles, E. S., Watson, C. S., Brun, F., Berthier, E., Esteves, M., Quincey, D. J., Miles, K. E., Hubbard, B., and Wagnon, P.: Glacial and  
563 geomorphic effects of a supraglacial lake drainage and outburst event, Everest region, Nepal Himalaya, *The Cryosphere*, 12, 3891–  
564 3905, <https://doi.org/10.5194/tc-12-3891-2018>, 2018.

565 Muñoz, R., Huggel, C., Frey, H., Cochachin, A., and Haeberli, W.: Glacial lake depth and volume estimation based on a large bathymetric  
566 dataset from the Cordillera Blanca, Peru, *Earth Surf. Process. Landf.*, <http://dx.doi.org/10.1002/esp.4826>, 2020.

567 Nie, Y., Liu, Q., Wang, J. D., Zhang, Y. L., Sheng, Y. W., and Liu, S. Y.: An inventory of historical glacial lake outburst floods in the  
568 Himalayas based on remote sensing observations and geomorphological analysis, *Geomorphology*, 308, 91–106,  
569 <https://doi.org/10.1016/j.geomorph.2018.02.002>, 2018.

570 Nie, Y., Liu, W., Liu, Q., Hu, X., and Westoby, M. J.: Reconstructing the Chongbaxia Tsho glacial lake outburst flood in the Eastern  
571 Himalaya: Evolution, process and impacts, *Geomorphology*, 370, 107393, <https://doi.org/10.1016/j.geomorph.2020.107393>, 2020.

572 O'Connor, J. E., Hardison III, J. H., Costa, J. E.: *Debris Flows from Failures of Neoglacial-Age Moraine Dams in the Three Sisters and*  
573 *Mount Jefferson Wilderness Areas, Oregon*, 105 pp, 2001.

574 Osti, R., and Egashira, S.: Hydrodynamic characteristics of the Tam Pokhari glacial lake outburst flood in the Mt. Everest region, Nepal,  
575 *Hydrol. Process.*, 23, 2943–2955, <http://dx.doi.org/10.1002/hyp.7405>, 2009.

576 Patel, L. K., Sharma, P., Laluraj, C. M., Thamban, M., Singh, A., and Ravindra, R.: A geospatial analysis of Samudra Tapu and Gepang  
577 Gath glacial lakes in the Chandra Basin, Western Himalaya, *Nat. Hazard*, 86, 1275–1290,  
578 <https://link.springer.com/article/10.1007/s11069-017-2743-4>, 2017.

579 Petrov, M. A., Sabitov, T. Y., Tomashevskaya, I. G., Glazirin, G. E., Chernomorets, S. S., Savernyuk, E. A., Tutubalina, O. V., Petrakov,  
580 D. A., Sokolov, L. S., Dokukin, M. D., Mountrakis, G., Ruiz-Villanueva, V., and Stoffel, M.: Glacial lake inventory and lake outburst  
581 potential in Uzbekistan, *Sci. Total Environ.*, 592, 228–242, <http://dx.doi.org/10.1016/j.scitotenv.2017.03.068>, 2017.

582 Qi, M. M., Liu, S. Y., Wu, K. P., Zhu, Y., Xie, F. M., Jin, H., Gao, Y. P. and Yao, X. J. Improving the accuracy of glacial lake volume  
583 estimation: A case study in the Poiqu basin, central Himalayas, *J. Hydrol.*, 610, <https://doi.org/10.1016/j.jhydrol.2022.127973>, 2022.

584 Rick, B., McGrath, D., Armstrong, W. and McCoy, S.W. Dam type and lake location characterize ice-marginal lake area change in Alaska  
585 and NW Canada between 1984 and 2019, *Cryosphere*, 16, 297–314. <https://doi.org/10.5194/tc-16-297-2022>, 2022.

586 Richardson, S. D., Reynolds, J. M.: An overview of glacial hazards in the Himalayas, *Quat. Int.*, 65–6, 31–47,  
587 [http://dx.doi.org/10.1016/S1040-6182\(99\)00035-X](http://dx.doi.org/10.1016/S1040-6182(99)00035-X), 2000.

588 Sakai, A.: Glacial lakes in the Himalayas: a review on formation and expansion processes, *Glob. Environ. Res.*, 16, 23–30, 2012.

589 Sattar, A., Haritashya, U. K., Kargel, J. S., Leonard, G. J., Shugar, D. H., and Chase, D. V.: Modeling lake outburst and downstream  
590 hazard assessment of the Lower Barun Glacial Lake, Nepal Himalaya, *J. Hydrol.*, 598, 126208.  
591 <https://doi.org/10.1016/j.jhydrol.2021.126208>, 2021.

592 Schneider, D., Huggel, C., Cochachin, A., Guillén, S., and García, J.: Mapping hazards from glacier lake outburst floods based on  
593 modelling of process cascades at Lake 513, Carhuaz, Peru, *Adv. Geosci.*, 35, 145–155, [http://dx.doi.org/10.5194/adgeo-35-145-](http://dx.doi.org/10.5194/adgeo-35-145-2014)  
594 2014, 2014.

595 Sharma, R. K., Pradhan, P., Sharma, N. P., and Shrestha, D. G.: Remote sensing and in situ-based assessment of rapidly growing South  
596 Lhonak glacial lake in eastern Himalaya, India, *Nat. Hazard*, 93, 393–409, <https://doi.org/10.1007/s11069-018-3305-0>, 2018.

597 Shugar, D. H., Burr, A., Haritashya, U. K., Kargel, J. S., Watson, C. S., Kennedy, M. C., Bevington, A. R., Betts, R. A., Harrison, S., and  
598 Strattman, K.: Rapid worldwide growth of glacial lakes since 1990, *Nat. Clim. Change*, 10, 939–945,  
599 <https://doi.org/10.1038/s41558-020-0855-4>, 2020.

600 Somos-Valenzuela, M. A., McKinney, D. C., Byers, A. C., Rounce, D. R., Portocarrero, C., and Lamsal, D.: Assessing downstream flood  
601 impacts due to a potential GLOF from Imja Tsho in Nepal, *Hydrol. Earth Syst. Sci.*, 19, 1401–1412, [http://dx.doi.org/10.5194/hess-](http://dx.doi.org/10.5194/hess-19-1401-2015)  
602 19-1401-2015, 2015.

603 Sugiyama, S., Skvarca, P., Naito, N., Enomoto, H., Tsutaki, S., Tone, K., Marinsek, S., and Aniya, M.: Ice speed of a calving glacier  
604 modulated by small fluctuations in basal water pressure, *Nat. Geosci.*, 4, 597–600, <http://dx.doi.org/10.1038/ngeo1218>, 2011.

605 Sugiyama, S., Minowa, M., Sakakibara, D., Skvarca, P., Sawagaki, T., Ohashi, Y., Naito, N., and Chikita, K.: Thermal structure of  
606 proglacial lakes in Patagonia, *J. Geophys. Res.: Earth Surf.*, 121, 2270–2286, <http://dx.doi.org/10.1002/2016JF004084>, 2016.

607 Sugiyama, S., Minowa, M., and Schaefer, M.: Underwater ice terrace observed at the front of Glaciar Grey, a freshwater calving glacier  
608 in Patagonia, *Geophys. Res. Lett.*, 46, 2602–2609, <http://dx.doi.org/10.1029/2018GL081441>, 2019.

609 Sugiyama, S., Minowa, M., Fukamachi, Y., Hata, S., Yamamoto, Y., Sauter, T., Schneider, C., and Schaefer, M.: Subglacial discharge  
610 controls seasonal variations in the thermal structure of a glacial lake in Patagonia, *Nat. Commun.*, 12, 1–9,  
611 <https://doi.org/10.1038/s41467-021-26578-0>, 2021.

612 Sutherland, J. L., Carrivick, J. L., Gandy, N., Shulmeister, J., Quincey, D. J., and Cornford, S. L.: Proglacial lakes control glacier  
613 geometry and behavior during recession, *Geophys. Res. Lett.*, 47, e2020GL088865, <https://doi.org/10.1029/2020GL088865>, 2020.

614 Veh, G., Korup, O., and Walz, A.: Hazard from Himalayan glacier lake outburst floods, *PNAS*, 117, 907–912,  
615 <https://www.pnas.org/cgi/doi/10.1073/pnas.1914898117>, 2020.

616 Wang, X., Liu, S. Y., Ding, Y. J., Guo, W. Q., Jiang, Z. L., Lin, J., and Han, Y.: An approach for estimating the breach probabilities of  
617 moraine-dammed lakes in the Chinese Himalayas using remote-sensing data, *Nat. Hazard Earth Syst. Sci.*, 12, 3109–3122,  
618 <http://dx.doi.org/10.5194/nhess-12-3109-2012>, 2012.

619 Wang, X., Guo, X. Y., Yang C. D., Liu, Q. H., Wei, J. F., Zhang, Y., Liu, S. Y., Zhang, Y. L., Jiang, Z. L., and Tang, Z. G.: Glacial lake  
620 inventory of high-mountain Asia in 1990 and 2018 derived from Landsat images, *Earth Syst. Sci. Data*, 12, 2169–2182,  
621 <https://doi.org/10.5194/essd-12-2169-2020>, 2020.

622 Wang, W. C., Gao, Y., Anaconda, P. I., Lei, Y. B., Xiang, Y., Zhang, G. Q., Li, S. H., and Lu, A. X.: Integrated hazard assessment of  
623 Cirenmaco glacial lake in Zhangzangbo valley, Central Himalayas, *Geomorphology*, 306, 292–305,  
624 <http://dx.doi.org/10.1016/j.geomorph.2015.08.013>, 2018.

625 Watson, C. S., Quincey, D. J., Carrivick, J. L., Smith, M. W., Rowan, A. V., and Richardson, R.: Heterogeneous water storage and thermal  
626 regime of supraglacial ponds on debris-covered glaciers, *Earth Surf. Process. Landf.*, 43, 229–241,  
627 <http://dx.doi.org/10.1002/esp.4236>, 2018.

628 Watson, C. S., Kargel, J. S., Shugar, D. H., Haritashya, U. K., Schiassi, E., and Furfaro, R. Mass Loss From Calving in Himalayan  
629 Proglacial Lakes *Front. Earth Sci.* 7, 342, <http://dx.doi.org/10.3389/feart.2019.00342>, 2020.

630 Westoby, M. J., Glasser, N. F., Brasington, J., Hambrey, M. J., Quincey, D. J., and Reynolds, J. M.: Modelling outburst floods from  
631 moraine-dammed glacial lakes, *Earth-Sci. Rev.*, 134, 137–159, <http://dx.doi.org/10.1016/j.earscirev.2014.03.009>, 2014.

632 Wood, J. L., Harrison, S., Wilson, R., Emmer, A., Yarleque, C., Glasser, N. F., Torres, J. C., Caballero, A., Araujo, J., Bennett, G. L.,  
633 Diaz-Moreno, A., Garay, D., Jara, H., Poma, C., Reynolds, J. M., Riveros, C. A., Romero, E., Shannon, S., Tinoco, T., Turpo, E.,  
634 and Villafane, H.: Contemporary glacial lakes in the Peruvian Andes, *Glob. Planet. Change*, 204, 103574,  
635 <https://doi.org/10.1016/j.gloplacha.2021.103574>, 2021.

636 Yao, T. D., Thompson, L., Yang, W., Yu, W. S., Gao, Y., Guo, X. J., Yang, X. X., Duan, K. Q., Zhao, H. B., Xu, B. Q., Pu, J. C., Lu, A.  
637 X., Xiang, Y., Kalltel, D. B., and Joswiak, D.: Different glacier status with atmospheric circulations in Tibetan Plateau and  
638 surroundings, *Nat. Clim. Change*, 2, 663–667, <http://www.nature.com/doi/10.1038/nclimate1580>, 2012.

639 Yao, T. D., Xue, Y. K., Chen, D. L., Chen, F. H., Thompson, L., Cui, P., Koike, T., K.-M. Lau, W., Lettenmaier, D., Mosbrugger, V.,  
640 Zhang, R. H., Xu, B. Q., Dozier, J., Gillespie, T., Gu, Y., Kang, S. C., Piao, S. L., Sugimoto, S., Ueno, K., Wang, L., Wang, W. C.,  
641 Zhang, F., Sheng, Y. W., Guo, W. D., Ailikun, Yang, X. X., Ma, Y. M., Shen, S. S. P., Su, Z. B., Chen, F., Liang, S. L., Liu, Y. M.,  
642 Singh, V. P., Yang, K., Yang, D. Q., Zhao, X. Q., Qian, Y., Zhang, Y., and Li, Q.: Recent third pole’s rapid warming accompanies  
643 cryospheric melt and water cycle intensification and interactions between monsoon and environment: Multidisciplinary approach  
644 with observations, modeling, and analysis, *B. Am. Meteorol. Soc.*, 100, 423–444, <https://doi.org/10.1175/BAMS-D-17-0057.1>,  
645 2019.

646 Yao, X. J., Liu, S. Y., Sun, M. P., Wei, J. F., and Guo, W. Q.: Volume calculation and analysis of the changes in moraine-dammed lakes  
647 in the north Himalaya: a case study of Longbasaba lake, *J. Glaciol.*, 58, 753–760, <http://dx.doi.org/10.3189/2012JoG11J048>, 2012.

648 Yao, X. J., Liu, S. Y., Han, L., Sun, M. P., and Zhao, L. L.: Definition and classification system of glacial lake for inventory and hazards  
649 study, *J. Geogr. Sci.*, 28, 193–205, <https://doi.org/10.1007/s11442-018-1467-z>, 2018.

650 Zemp, M., Huss, M., Thibert, E., McNabb, R., Huber, J., Barandun, M., Machguth, H., Nussbaumer, S. U., Gärtner-roer, I., Thomson,  
651 L., Paul, F., Maussion, F., Kutuzov, S., and Cogley, J. G.: Global glacier mass changes and their contributions to sea-level rise from  
652 1961 to 2016, *Nature*, 568, 382–386, <https://doi.org/10.1038/s41586-019-1071-0>, 2019.

653 Zhang, G. Q., Yao, T. D., Xie, H. J., Wang, W. C., and Yang, Wei.: An inventory of glacial lakes in the Third Pole region and their changes  
654 in response to global warming, *Glob. Planet. Change*, 131, 148–157, <http://dx.doi.org/10.1016/j.gloplacha.2015.05.013>, 2015.

655 Zhang, G. Q., Bolch, T., Yao, T. D., Rounce, D.R., Chen, W. F., Veh, G., King, O., Allen, S.K., Wang, M. and Wang, W. C. Underestimated  
656 mass loss from lake-terminating glaciers in the greater Himalaya, *Nat. Geosci.*, 16, 1–6. [https://doi.org/10.1038/s41561-023-01150-](https://doi.org/10.1038/s41561-023-01150-1)  
657 1, 2023.

658 Zhang, T. G., Wang, W. C., Gao, T. G., and An, B. S.: Simulation and Assessment of Future Glacial Lake Outburst Floods in the Poiqu  
659 River Basin, Central Himalayas, *Water*, 13, <https://doi.org/10.3390/w13101376>, 2021.

660 Zhang, T. G., Wang, W. C., An, B. S., Gao, T. G., and Yao, T. D.: Ice thickness and morphological analysis reveal the future glacial lake  
661 distribution and formation probability in the Tibetan Plateau and its surroundings, *Glob. Planet. Change*, 216, 103923,  
662 <https://doi.org/10.1016/j.gloplacha.2022.103923>, 2022.

663 Zheng, G. X., Mergili, M., Emmer, A., Allen, S., Bao, A. M., Guo, H., and Stoffel, M.: The 2020 glacial lake outburst flood at Jinwuco,  
664 Tibet: causes, impacts, and implications for hazard and risk assessment, *The Cryosphere*, 15, 3159–3180, [https://doi.org/10.5194/tc-](https://doi.org/10.5194/tc-15-3159-2021)  
665 15-3159-2021, 2021.